LATE HOLOCENE CLIMATE INFERRED FROM VARVED SEDIMENTS, BLUE LAKE, BROOKS RANGE, ALASKA

by

Barbara Gabriele Osgood

B.S. in Environmental Geology, Indiana University of Pennsylvania, 1997

Submitted to the Graduate Faculty of

Arts and Sciences in partial fulfillment

of the requirements for the degree of

M.S. in Geology

University of Pittsburgh

2004

UNIVERSITY OF PITTSBURGH

FACULTY OF ARTS AND SCIENCES

This thesis was presented

by

Barbara Gabriele Osgood

It was defended on

August 19, 2004

and approved by

Michael Rosenmeier, PhD, Assistant Professor

Charles Jones, PhD, Assistant Professor

Thesis Director: Mark B. Abbott, PhD, Assistant Professor

LATE HOLOCENE CLIMATE INFERRED FROM VARVED SEDIMENTS IN BLUE LAKE, BROOKS RANGE, ALASKA

Barbara Gabriele Osgood, M.S.

University of Pittsburgh, 2004

Geomorphologic evidence provided by late Holocene glacial advances demonstrates the sensitivity of central Brooks Range to changes in temperature and moisture balance over decadal to centennial timescales. High-resolution climate proxy records covering the middle to late Holocene are sparse from this region. One exception is Blue Lake, a small (<0.5 km^2), shallow (4.7 m), glacier-fed lake set on the crest of the Brooks Range (68º05.3' N, 150º27.8' W) in north-central Alaska at an altitude of 1265 m. The 4 km^2 watershed contains a small cirque glacier located on the north face of the 1890 m high headwall, on the north side of the continental divide. Field observations and air photos indicate that melt-water from the glacier contributes a substantial quantity of fine-grained sediment to the lake. Sediment cores recovered in August of 1999 contain millimeter-scale laminations comprised of lamina couplets, which exhibit the classic mode of varve formation in a glacial basin consisting of a succession of fine sands to silts deposited during the summer months, followed by a well-defined winter clay cap. In addition to annual variability in varve thickness, long-term trends in thickness were identified and compared with the historical climate record. Blue Lake records the glacial response to late Holocene climate phenomena, such as the Little Ice Age (cooling), Medieval Climatic Anomaly (warming), and the 20th century warming trend.Varve measurements from Blue Lake correlate well with regional cooling and warming trends described for the late Holocene from other proxy records across the Arctic.

ACKNOWLEDGEMENTS

I would like to express my sincerest thanks to the following people that helped make this thesis possible. This endeavor would not have been possible without their support and encouragement.

First, to Mark Abbott, my advisor, for giving me the means, motivation and inspiration to make it through this project and for all that I have learned…

To my committee members Mike Rosenmeier and Charlie Jones for all the time they spent assisting me with this project, for their support, many discussions, and, of course, all the technical assistance and revisions….

To all my friends in the Department of Geology and Planetary Science, both students and staff.

A special thanks to Dolly Chavez and Deanna Hitchcock for all their administrative assistance (I would have been lost without you)…. to Lara Homsey and Danielle Deemer, for their friendship and encouragement. You were both an inspiration to me… and to Dan Nelson and Nathan Stansell for too many things to list.

To my family (mom, dad, Barb and Jim) for their moral support (and babysitting) when I needed it the most…

And most of all, I would like to thank my husband, Tom

For his patience, understanding, encouragement, and especially for believing in me…

TABLE OF CONTENTS

LIST OF TABLES

LIST OF FIGURES

1.0 INTRODUCTION

General circulation models (GCM) and paleoclimate records suggest that the high northern latitudes are sensitive to changes in global controls of the climate system, such as insolation and atmospheric greenhouse gases (Bartlein et al., 1992; Wright et al., 1993; MacDonald et al., 2000; IPCC, 2001). As a result, global climate change may be first recognized in the Arctic. Model results suggest that future global warming is likely to be amplified in high latitude regions as a result of feedback effects. For example, feedback effects associated with the albedo of snow and ice covered surfaces can amplify small shifts in temperature (Overpeck et al., 1997; MacDonald et al., 2000). Changes in sea ice and snow cover affects middle and low-latitude climate by altering circulation systems and oceanic transport of heat from low latitudes. Input of cold freshwater into the North Atlantic from glacial meltwater and high rates of iceberg calving could alter the pattern and rate of deep-water formation, and thereby alter thermohaline circulation, and global heat transport. In addition, the equator-pole temperature gradient is directly influenced by Arctic conditions by affecting patterns and intensity of atmospheric circulation over the Northern Hemisphere (IPCC, 2001). Whitfield et al. (2004) suggested that shifts in climate patterns will affect hydrologic and ecological processes in the Arctic and that those impacts will contribute to shifts in regional and global climate mechanisms. These shifts in Arctic climate will likely have profound ecological, social, and economic implications (Whitfield et al., 2004).

Reconstructions (Mann et al., 1999) of 20th century Northern Hemisphere mean temperatures suggest that the last century was exceptional in both the rate and magnitude of temperature increase. Recent studies show that Arctic temperature and precipitation have increased during the 20th century (IPCC, 2001). Evidence of mild episodes in the 11th and 12th centuries exist, however, mean temperature was not comparable to those of late 20th century levels (Mann et al., 1999). Anthropogenic effects on future climate, whatever they may be, will be superimposed on an underlying background of variability which varies on different time scales in response to numerous forcing factors (Bradley, 2000). Background climate variability cannot be determined from the short instrumental record because of its short duration and poor spatial coverage. Although GCM's suggest Arctic sensitivity, there are few instrumental meteorological records that extend past the mid-19th century, limiting the ability to evaluate mechanisms driving climate change (Lamoureux et al., 2004). The ability to forecast future climate change relies on knowledge of past climate changes. In order to put potential future greenhouse warming in perspective we need to define the range of natural variability by reconstructing paleoclimate records from climate proxies (Bradley, 2000).

Here a >1000-year record of summer temperatures from the Brooks Range of Alaska is reconstructed from varved sediments. Blue Lake is a proglacial system located in the Arctic region of Alaska (68º05.3 N, 150º27.8 W) that contains annually laminated sediments represented by couplets of silt (summer-layer) and clay (winter-layer). The climate record produced at this site is compared to other proxy records from the Arctic in order to assess the geographic distribution of climate shifts during the last 1000 years.

1.1 PALEOCLIMATE PROXIES

Climate archives are available from a variety of environmental sources that are sensitive to environmental change, such as tree rings, corals, ice cores, lake sediments and marine deposits (Bradley and Jones, 1992). Annually laminated lake sediments (varved) hold particular promise in the study of high latitude environments, because climatic variability can be resolved year by year. During the spring and summer, high latitude lakes receive nival discharge, dominated by silt-sized inorganic material, followed by ice cover during the fall and winter, when clay-sized particles are deposited. Summer temperatures strongly influence streamflow velocity and suspended sediment content leading to temperature-dependent variations in summer-layer thickness, with warmer summers forming thicker layers and cooler summers thinner layers (Hardy, 1996). Arctic lakes are sensitive sites for paleoclimate reconstruction, because they are remote with limited human impact, spring and summer rainfall is rare, and the period in which runoff occurs is limited (Lemmen, 1989; Hughen et al., 2000; Lamoureux, 2000; Francus et al., 2002b; Lamoureux et al., 2004).).

1.2 ANNUALLY LAMINATED LAKE SEDIMENTS

A varve consists of a coarse-grained summer-layer usually composed of silt-sized mineral matter overlain by a winter-layer of clay-sized sediment formed during low energy conditions under the winter ice cover. Varve preservation occurs only if there are no post-depositional disturbances of the sediment surface which is generally the case in deep lakes that are topographically protected from mixing. Various limnological and hydrological processes controlled by individual watersheds and lake basins determine the composition, structure and thickness of varves. Varves at lower latitudes may contain layers of calcite, deposited in the summer and termed *calcareous*. Layers formed under seasonal variations in redox conditions are called *ferrogenic*, layers consisting of diatoms or other algae are termed *biogenic*, and layers composed primarily of allochthonous material are termed *clastic* varves (O'Sullivan, 1983; Saarnisto, 1986; Zolitschka, 1996a). Varves may be summarized as local biological, geochemical and sedimentological responses to one or more forcing factors. Climate variations directly influence a multitude of lake and catchment processes including geomorphological processes, such as weathering, erosion and transportation, soil development, and vegetation (Zolitschka, 1996a). A distinct relationship between the structure, composition and thickness of varves with environmental conditions and climate changes exists. Annually laminated sediments have been applied to a variety of studies such as paleoclimatology, vegetation history, rates of sediment accumulation, rates of pollutant influx, as well as geochronology (O'Sullivan, 1983).

Several factors need to be considered in order to validate a varve chronology in lake sediments. First, the varve structure must be determined and the formation processes understood. Second, the sediment samples and sub-samples must be undisturbed. Third, the varve chronology must be validated with an independent dating method (Ojala et al., 2003). Varves, originally used primarily as a stratigraphic tool, have become an important indicator of past climate and environmental conditions with high time resolution (Leeman and Niessen, 1994). This study will focus on the conditions controlling the formation of proglacial clastic varves, their internal structure, composition, and relationship to paleoenvironmental conditions.

1.3 PROGLACIAL VARVES

Lakes containing annually laminated sediments are generally associated with thermally stratified water columns (O'Sullivan, 1983). Thermally stratified water columns promote varve formation by causing interflows and suspension settling. Interflows occur when sediment-laden stream water enters a lake. This stream water has a greater density than the relatively warm surface water causing it to sink and flow along the lake bottom to the until it reaches the thermocline where it meets cold water with a greater density causing the inflowing water to flow along the top of the thermocline resulting in suspension settling. Additionally, thermally-stratified lakes result in isolation of the hypolimnion and the formation of undisturbed sediments (O'Sullivan, 1983). However, varves may also be formed in lakes with unstratified water columns such as Blue Lake (Sturm, 1979). Here the high sedimentation influx is so great due to high weathering rates of the soft red-shale bedrock that it produces couplets of coarse-grained material (spring/summer-layer) overlain by a clay cap (winter-layer). Varves formed in this manner are composed primarily of allochthonous material (O'Sullivan, 1983; Zolitschka, 1996a). According to Sturm (1979), clastic varves are a result of seasonal sediment influx to the lake. The seasonal or discontinuous influx will form varves of the classic bimodal structure described by de Geer (1912). The sediments comprising clastic varves may also exhibit seasonal variation in particle size as well as other qualitative and quantitative characteristics (O'Sullivan, 1983).

Clastic varves are formed in lakes with a high influx of minerogenic matter. A distinction can be made between proglacial lakes and other lakes with clastic varves. Varves formed in glaciolacustrine environments are rich in allochthonous minerogenic matter (Saarnisto, 1986) and exhibit influx of silt- and clay-sized material which is clearly linked to the physical weathering and erosion of glaciers (Zolitschka, 1996a). The classic mode of varve formation in a glacial basin consists of a succession of fine-sands to silts deposited during the summer months, followed by a well-defined winter clay cap (De Geer, 1912; O'Sullivan, 1983; Leeman and Niessen, 1994; Zolitschka, 1996a; Lamoureux and Bradley, 1996; Lamoureux, 1999). The cold and arid Arctic climate of the Brooks Range limits above freezing temperatures to three to four months during the late spring and summer. Warming temperatures during the spring and summer months produce a melt season with an influx of terrigenous fine sands and silts as a result of snowmelt and glacier runoff (Hardy, 1996). This early melt may last only a couple of weeks to a month but is responsible for the transfer of up to 90% of the sediment to the lake (Hardy, 1996; Zolitschka, 1996a). In glaciated basins, the influx of sediment may be limited to discharge peaks early in the melt season. For example, Ostrem et al. (1967) observed that approximately 60% of the annual sediment load was transported to a glaciated basin on Baffin Island in a single day. On northern Ellesmere Island, a pattern was observed where 34% and 84% of the annual sediment flux was transported in three days and the first month of the melt season, respectively (Hardy, 1992). After the initial melt, the flux of runoff and available energy of transport decreases and the size of grains transported into the lake becomes finer. The outcome of reduced energy is a fining upward sequence. Late season rainfall events may increase runoff but sediment transfer remains negligible as long as rainfall discharge does not exceed the snowmelt and glacial runoff flood (Hardy, 1996).

Arctic climate assures that during the winter lake surfaces are frozen, thus interrupting all sediment influx. The winter ice cover enables fine clay-sized material suspended in the water column to settle to the bottom forming an independent layer which appears in thin section as a dark lamina (Lamoureux, 1999). Varve identification is dependent on the formation of that winter clay cap after sediment inflow has ceased. The resulting varve couplets typically appear as millimeter-scale, normally graded units of sand, silt and clay separated by sharp, conformable contacts (Lamoureux, 1999).

1.4 CLIMATE-VARVE RELATIONSHIPS

1.4.1 Calibration

In order to use varve thickness as a proxy for summer temperatures it is essential to know the relationship between sediment supply and summer temperature (Hardy et al., 1996). This is accomplished by making statistical correlations among sediment supplied by inflowing rivers, summer layer thickness, and meteorological data. The technique is analogous to that of dendroclimatic reconstructions in which thickness measurements are first standardized and then calibrated with the instrumental record. Once established, this climate-varve relationship determined for the calibrated period can be used for the entire record if past conditions of the lake and catchment area are constant for the time span covered by the sediment core (Zolitschka, 1996a).

1.4.2 Paleoclimate controls

Understanding the mechanisms of sediment flux and the conditions of varve formation is essential for interpreting paleoenvironmental conditions (Hardy et al., 1996; Zolitschka, 1996a). Controlling factors influencing varve thickness includes solar radiation, spring/summer temperature, and precipitation. Temperature and precipitation data are available from many weather stations. Most studies in the Arctic have concluded that proglacial varve formation is primarily controlled by runoff related to summer temperature (Zolitschka, 1996a, 1996b). Runoff in regions with high summer irradiance and negligible precipitation primarily depends on snowmelt from both winter accumulation and glacial retreat. Melting is related to summer temperature or irradiance by an index of available energy that controls ice and snow ablation rates (Leonard, 1986; Leeman and Niessen, 1994; Hardy, 1996; Desloges, 1994). Zolitschka (1996a) concluded that temperature is the primary influence while precipitation is of minor or no importance.

Previous studies of clastic varve thickness from glacier-fed lakes show a strong correlation between annual sediment accumulation and average snowmelt season temperatures (Leonard, 1986, 1997; Leeman and Neissen, 1994; Hardy et al., 1996; Zolitschka, 1998; Hughen et al., 2000; Moore et al., 2001). Hardy et al., (1996) established that the thickness and composition of clastic varves in Lake C2, Ellesmere Island, were controlled by sediment discharge that was dependent on summer temperatures. Lake C2 is a glacial-fed system and therefore snowmelt is not a limiting factor given the “endless” supply of potential melt water. Varve thickness was correlated with average summer temperatures in Upper Soper Lake, Baffin Island, Canada (Hughen et al., 2000) and in Donard Lake, Baffin Island, Canada (Moore et al., 2001). Again, thickness measurements were used to reconstruct average summer paleotemperatures. Leonard (1986; 1997) observed that glacial melt controls the rate of sedimentation of glacier-fed Hector Lake. Studies investigating the relation between runoff and varve thickness in glacier-fed lakes indicate that varve thickness is correlated to the amount of inflowing meltwater, which is controlled by temperature or precipitation (Zolitschka, 1996a).

In many varve records there exits variability that cannot be explained by changes in summer temperature (Hardy, 1996). This degree of unexplained variability is attributed to other factors that influence sedimentation such as hydrometeorologic (rainfall events), hydrologic (sediment flushing from fluvial storage), and non-climatic processes (subaqueous slumping or ice-dammed lake drainage) (Lamoureux, 2000). For example, intense arctic rainfall events during the summer months when the lake is ice-free may produce high runoff, sediment erosion and increased suspended sediment loads into arctic lakes (Hardy, 1996; Lamoureux, 2000). Sediment erosion may occur as a result of runoff on poorly vegetated slopes, gullying, localized earth flows, and primarily a result of channel bank erosion and remobilization of floodplain sediments during high river stage (Lamoureux, 2000). Winter precipitation may influence the amount of discharge and, in turn, the amount of sediment flux during the following summer (Moore et al., 2001). The initial pulse of spring melt can become ponded behind temporary dams of ice or wind-drifted snow. When the temporary dams fail drainage occurs rapidly. In addition, the spring melt may reach the lake while it is still ice covered. In this case, discharge is prevented from entering the lake and spreads on top of the lake ice until the ice edge melts (Lamoureux, 2000).

1.5 INDEPENDENT DATING TECHNIQUES

Varved sediment records provide an absolute chronology for paleoenvironmental reconstructions. Absolute dating is critical for high-resolution paleoclimatic constructions because it provides a precise age control for calibration of proxy data with instrumental records.

Nonetheless, varve chronologies need verification by independent dating methods since finely laminated sequences can contain either extra or missing layers (Zolitschka, 1996a). High elevation Arctic lakes often contain little or no organic matter suitable for radiocarbon dating. Therefore, verifying a varve chronology is complicated when radiocarbon dating is not a viable option (Moore et al., 2001). The use of the radionuclides ^{210}Pb and ^{137}Cs has enabled dating of sediments for the last 100 years allowing the calculation of sedimentation rates (Appleby et al., 1998). Additionally, volcanic eruptions can be used as stratigraphic markers if dated at other localities and correlation is possible (Zolitschka, 1996a).

^{210}Pb is one of the last elements created by the decay of ^{238}U. ^{210}Pb forms naturally in rocks and sediments that contain ^{238}U and is found naturally in the atmosphere as a by-product of radon gas. ^{210}Pb has a decay constant of 0.03114 yr^{-1}, a half-life of 22.26 years and reaches near-zero radioactivity in ~7 half-lives or 150 years. It should be recognized that ^{210}Pb adsorbs rapidly onto particulate matter and may become mobile during sediment resuspension or redeposition (Binford et al., 1993).

The severe environmental conditions of the Arctic influence the behavior of atmospheric radionuclides in lake sediments by delaying production and transport due to nine or more months of ice cover. Permafrost suppresses the escape of gaseous ^{222}Rn from soils resulting in reduced atmospheric ^{210}Pb flux in Arctic lakes as compared to temperate lakes (Hermanson, 1990). Most atmospheric ^{210}Pb in the Arctic comes from lower latitudes and may rely on stratosphere-troposphere exchange processes (Wolfe et al., in press). There is also a correlation between the decline in ^{210}Pb and ^{137}Cs fallout values associated with declining precipitation amounts north of 50˚N latitude (Hermanson, 1990).

2.0 STUDY AREA

2.1 LOCATION

Blue Lake (68º05.3′N, 150º27.8′W) is located in the Chandler Lake quadrangle (A-1) on the northern slope of the Brooks Range off of Haul Road (Dalton Highway) and north of the east-west trending Continental Divide (Figure 2.1). Blue Lake is situated in the Arctic climate zone within the zone of permafrost and tundra, both north and above the boreal spruce forest. The continental divide between the Pacific and Arctic oceans corresponds with the climate transition zone between the continental climate of Alaska's interior and the cooler Arctic regime of the North Slope (Ellis and Calkin, 1984). Blue Lake is a flat bottom, glacier-fed lake 4.6 m deep with an area of 0.056 km^2 and located at an elevation of 1265 m (Figure 2.2). Air photos and field observations indicate that melt-water from the glacier contributes a substantial quantity of fine-grained sediment to the lake (Figure 2.3). On color infrared air photos, Blue Lake appears bright blue because of fine-grained sediment whereas lakes with low silt concentrations appear black. Comparisons of air photos from 1970 AD and 1979 AD show a rapid retreat (Figures 2.4a and b).

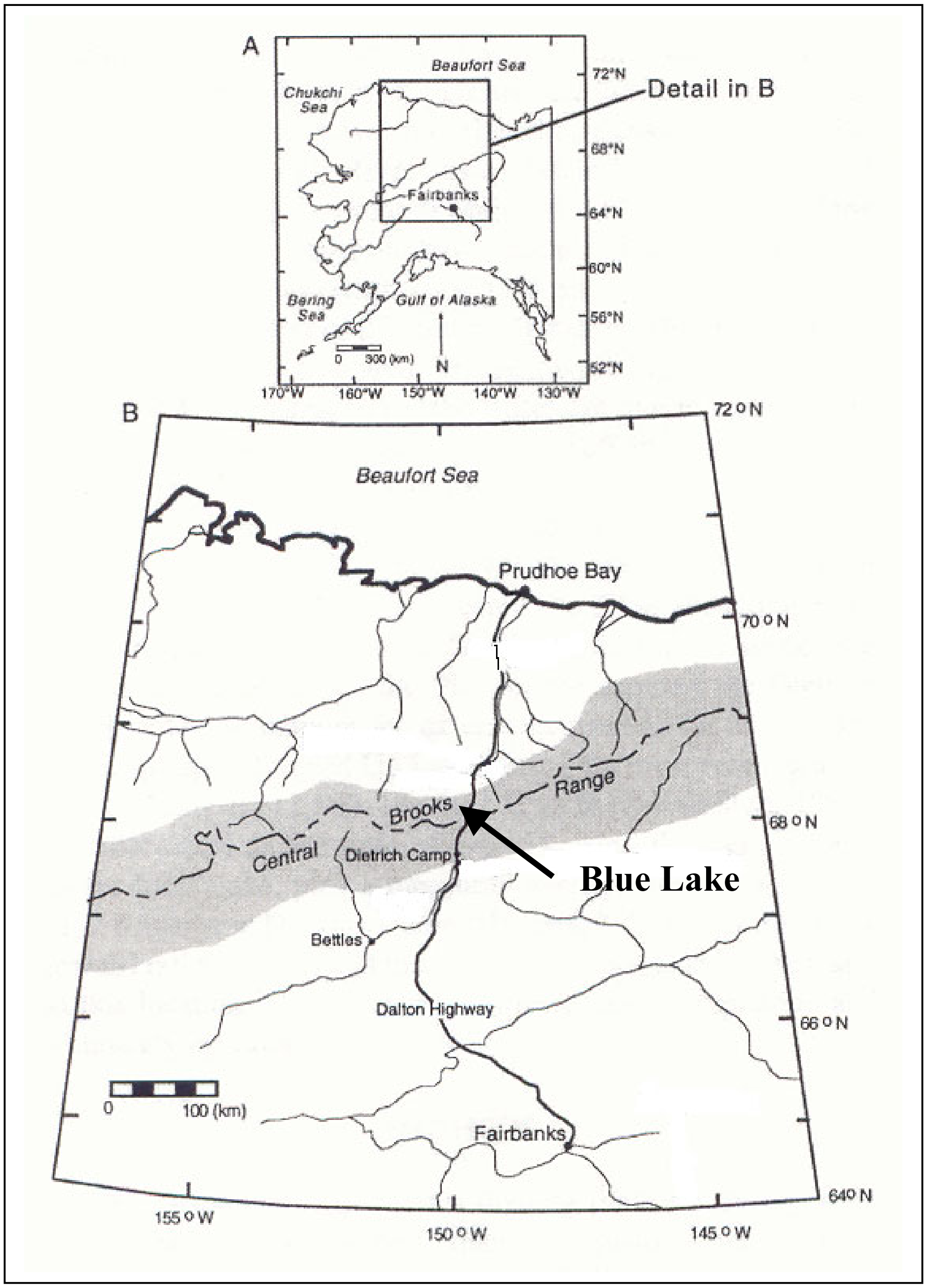

Figure 2.1: Location of Blue Lake (modified from Haugen, 1982).

Figure 2.2: Blue Lake, 1999 AD field season.

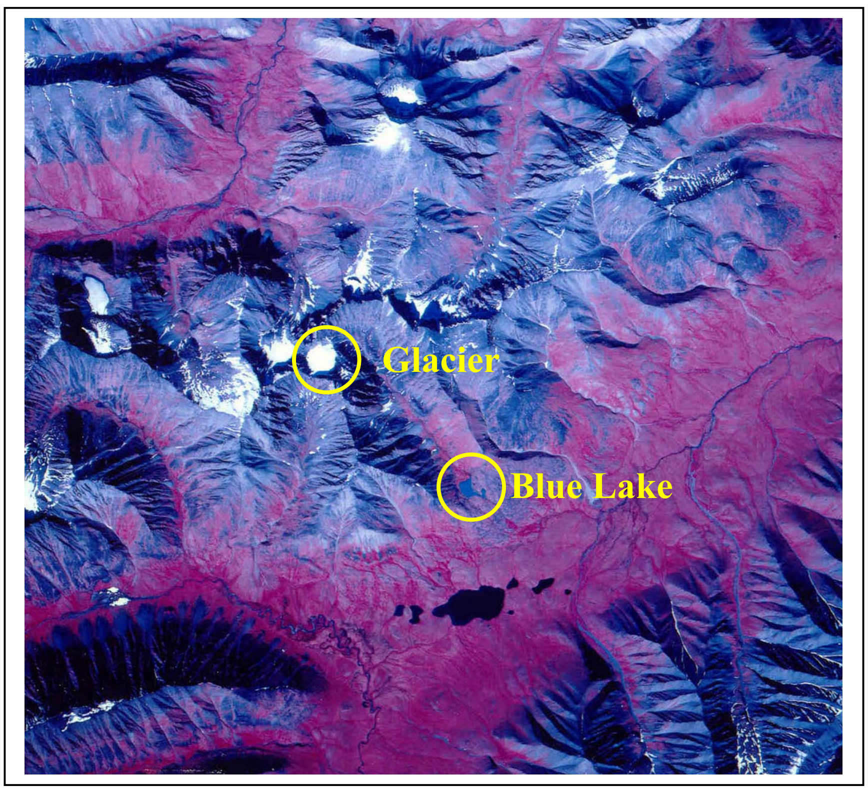

Figure 2.3: High altitude color infrared air photo showing cirque glacier and Blue Lake.

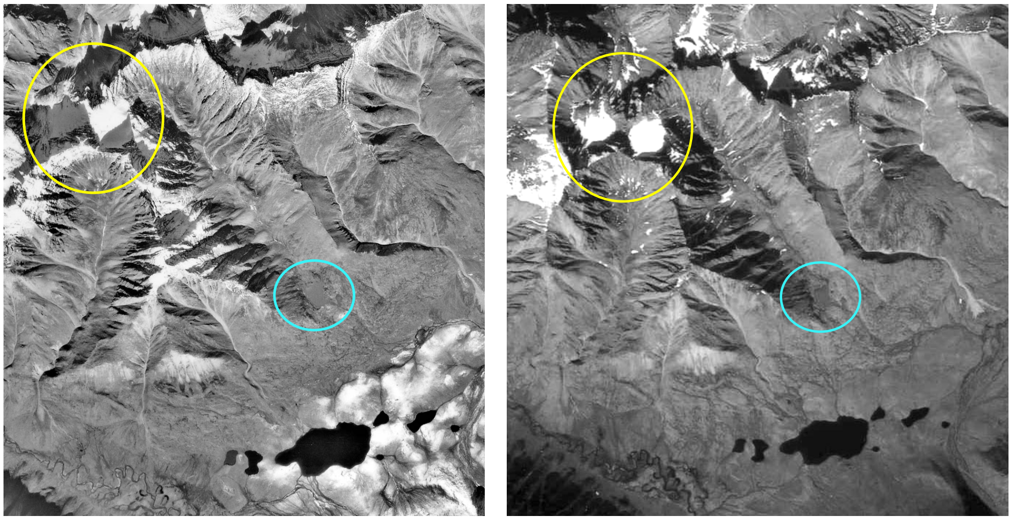

August 31, 1970 AD July 12, 1979 AD

Figure 2.4: Air photos of the Blue Lake glacier showing a rapid retreat since 1970.

2.2 CLIMATE

Alaska is divided into four climatic regions: maritime, continental, transitional maritime-continental, and arctic (Figure 2.5, Table 2.1). The present Alaskan climate is a result of interacting Arctic, cool Pacific, and mild Pacific air-masses (Table 2.1) (Anderson and Brubaker, 1993).

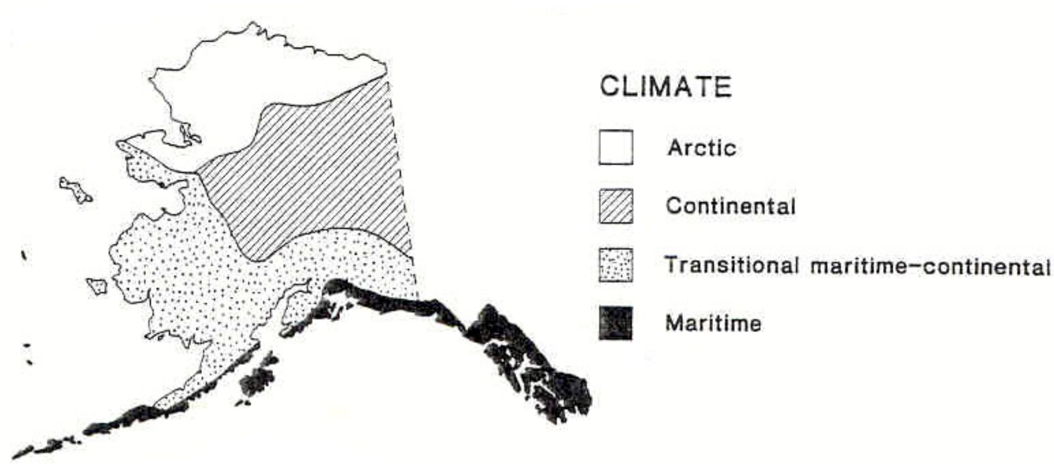

Figure 2.5: Alaska's four climate regions (modified from Anderson and Brubaker, 1993).

Table 2.1: Mean annual and seasonal temperature and precipitation ranges for the four Alaskan climate regions (modified from Anderson and Brubaker, 1993).

	Arctic	Continental	Transitional	Maritime
mean annual temperature (ºC)	-12.7 to -7	-7.5 to -2.5	-5 to +2.5	2.5 to 5
mean January temperature (ºC)	-27.5 to -20	-27.5 to -20	-20 to -10	-10 to -2.5
mean July temperature (ºC)	5 to 12.5	12.5 to 15	10 to 12.5	10 to 12.5
mean annual precipitation (mm)	<8 to 16	<8 to 16	16 to 24	24 to >160
mean January precipitation (mm)	<10 to 25	<10 to 25	25 to 100	100 to >200
mean July precipitation (mm)	25 to 75	25 to 100	50 to 100	100 to 150

The east-west trending Brooks Range exceeds 3500 m elevation and has a significant effect on regional climate. The climate of Alaska is generally topographically controlled with total precipitation decreasing at higher latitudes (Mock et al., 1998). Arctic air-masses dominate the winters of the interior and northern Alaska, bringing cold and dry conditions to the region. The Arctic front shifts northward during the summer to a position over the Brooks Range. This allows mild, moist Pacific air to flow into the Alaskan interior (Bryson, 1974). Weak cyclonic systems originating in Siberia over the Arctic Ocean move along the front becoming additional sources of summer precipitation. South of the Arctic front summers are relatively warm and wet. North of the Arctic front, the dominance of the Arctic air-masses and the cold Beaufort and Chukchi Seas keep summers cool. The Arctic climate zone is characterized by relatively low precipitation throughout the year (Anderson and Brubaker, 1993).

The geographic range of Alaska is extensive: 586,400 square miles and almost 20º of latitude. There are 21 First-Order weather stations in Alaska that represent observations taken by weather service personnel (Figure 2.6). First-order stations are those that are maintained by the National Weather Service (NWS) or the Federal Aviation Administration. Cooperative Observing Stations are a part of the U.S. Cooperative Observing Network in which observations are taken by local volunteers trained by the NWS. One cooperative station located near Blue Lake with sufficient data coverage was Umiat (69º 22' N, 152º 08' W).

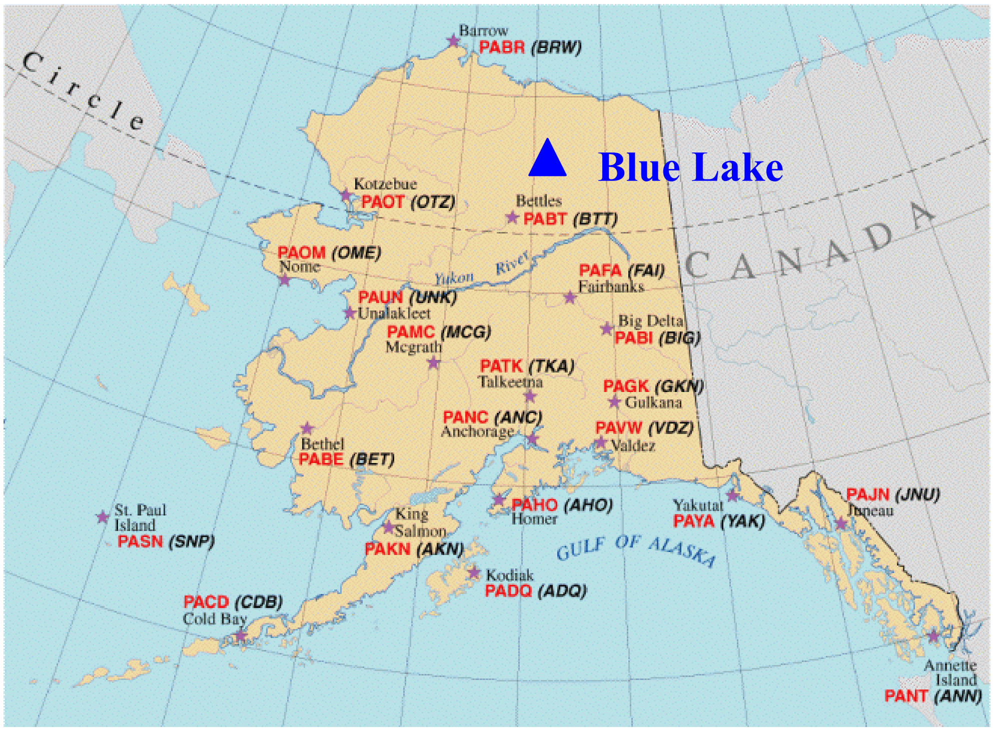

Figure 2.6: First-Order National Weather Service Stations (www.climate.gi.Alaska.edu).

The only First-Order station located in the Arctic region, Barrow (71º 17'N, 156º 46'W), is situated on the northern coast of Alaska, 8 m above sea level. Temperatures remain below freezing throughout most of the year (Figure 2.7). February is the coldest month and July is the warmest month of the year with temperatures averaging –27.33°C and 4.27°C, respectively. The month of May represents a transition from winter to summer and late-August to early September typically brings the end of the summer to the area. Umiat (69º 22' N, 152º 08' W), a cooperative station located in the Arctic region, elevation of 81 m, shows similar temperature variations to Barrow. May is the transition month from winter to summer and the end of summer coincides with late-August and early-September. Temperatures remain below freezing for most of the year (approximately nine months). July is the warmest month of the year with an average temperature of 11.38°C. Located in the Interior region of Alaska, Bettles (66º 55'N, 151º 31'W) is situated near the Koyukuk River, adjacent to the Endicott Mountains, 196 m above sea level. The summer days are long and temperatures are generally mild with maximum daily averages in the high 10’s and 20’s (ºC). Temperatures in the winters reach averages below freezing from October to April. June and July are the warmest months of the year with average temperatures of 13.97°C and 15.11°C. April represents a transition from winter to summer while September brings an end to summer in the region. The transition from winter to summer (and vice versa) is rapid in the Alaskan interior climate region resulting in short spring and fall seasons. Fairbanks (64º 49'N, 147º 51'W) is located in the Tanana Valley at an elevation of 132 m and has a typical continental climate. During June and July maximum average daily temperatures generally reach the lower 20’s (ºC). The transition from winter to summer generally occurs in April while September brings the beginning of the winter season. A large range in temperature variation during the winters in the Interior region is a result of cold weather brought on by dry, northerly airflow from the Arctic to mild weather associated with southerly airflow from the Gulf of Alaska. As seen in the plots, total precipitation decreases with increasing latitude (Figure 2.8). Monthly average precipitation graphs for Barrow, Umiat, and Bettles demonstrate that precipitation peaks in late summer, quickly rising from a minimum in early spring to a maximum in August.

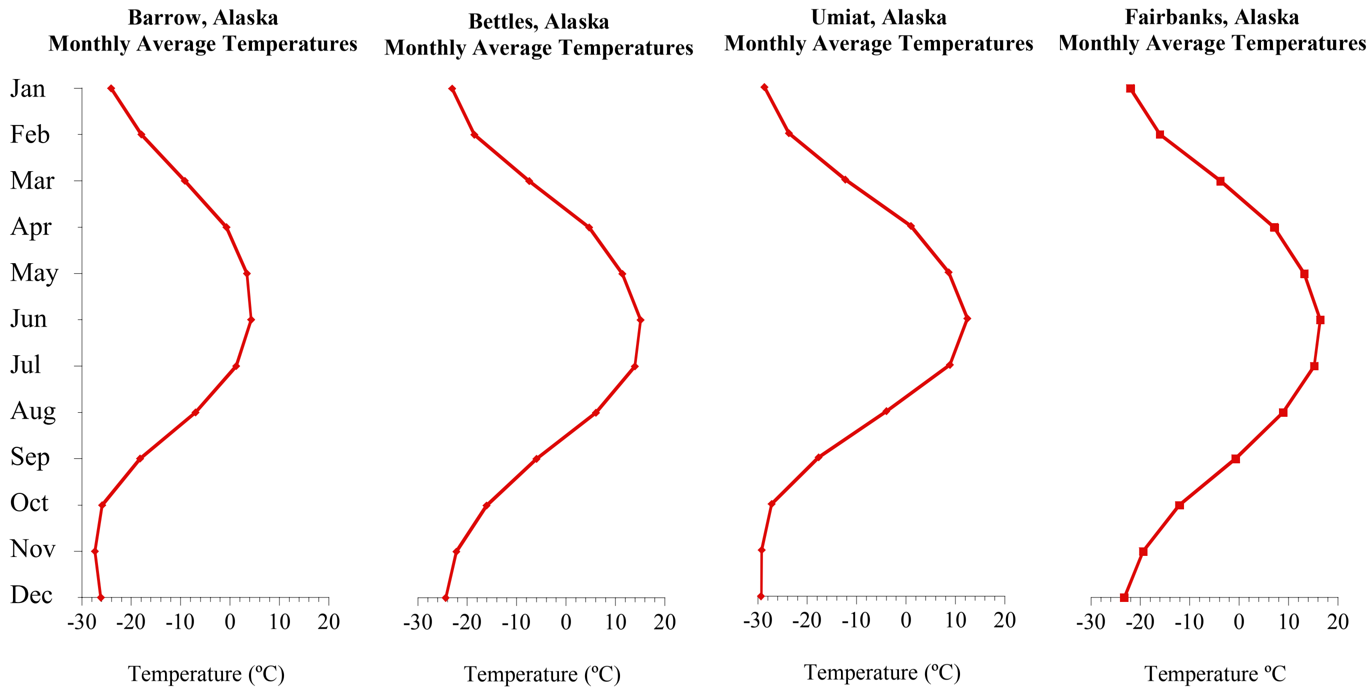

Figure 2.7: Monthly mean temperatures for select Alaskan meteorological stations.

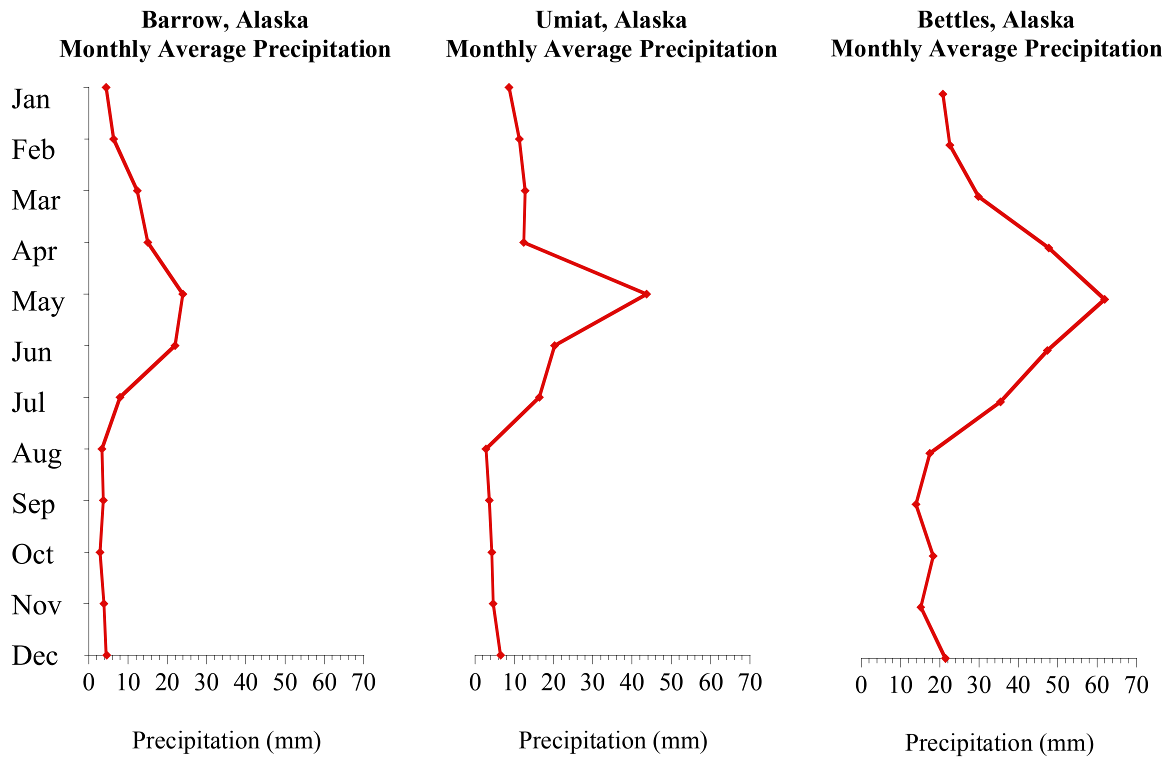

Figure 2.8: Monthly average precipitation for select Alaskan meteorological stations.

Instrumental records from three weather stations in Alaska show annual warming trends, particularly in the spring and winter (Table 2.2, Figure 2.9) with the most significant mean annual warming in Barrow and the least amount of warming in Fairbanks. Fairbanks recorded mean summer temperatures exhibit a brief warming in the early 1940's and the late 1950's. Summer temperatures are cooler from the late 1950's until the mid-1960, followed by another warming. The warming is most dramatic following the 1970's. The Fairbanks record shows an abrupt shift into the warmest period of the recorded data from approximately 1974 AD through 1994 AD, followed by a slight cooling trend. Umiat and Barrow also show an abrupt warming trend but does not show signs of a post 1990's cooling. Barrow continues its warming trend while Umiat shows a pronounced shift into a cold period during the early to mid-1980. Mean annual summer temperature records also show a post-1970's warming trend (Figure 2.10). However, summer temperature records show an abrupt shift to a cool interval in the early 1980's, followed by a shift to another warm interval in the late 1980's. This shift is more pronounced at Fairbanks and Bettles (Interior Alaska). Precipitation trends have been variable (Figure 2.11).

Table 2.2: Mean annual and seasonal temperature changes (www.climate.gi.alaska.edu).

Location	Annual	Spring	Summer	Autumn	Winter
Barrow	+4.16	+6.97	+2.78	+3.74	+2.94
Bettles	+2.59	+4.83	-0.08	-0.58	+4.93
Fairbanks	+1.07	+3.55	-0.05	-2.50	+3.05

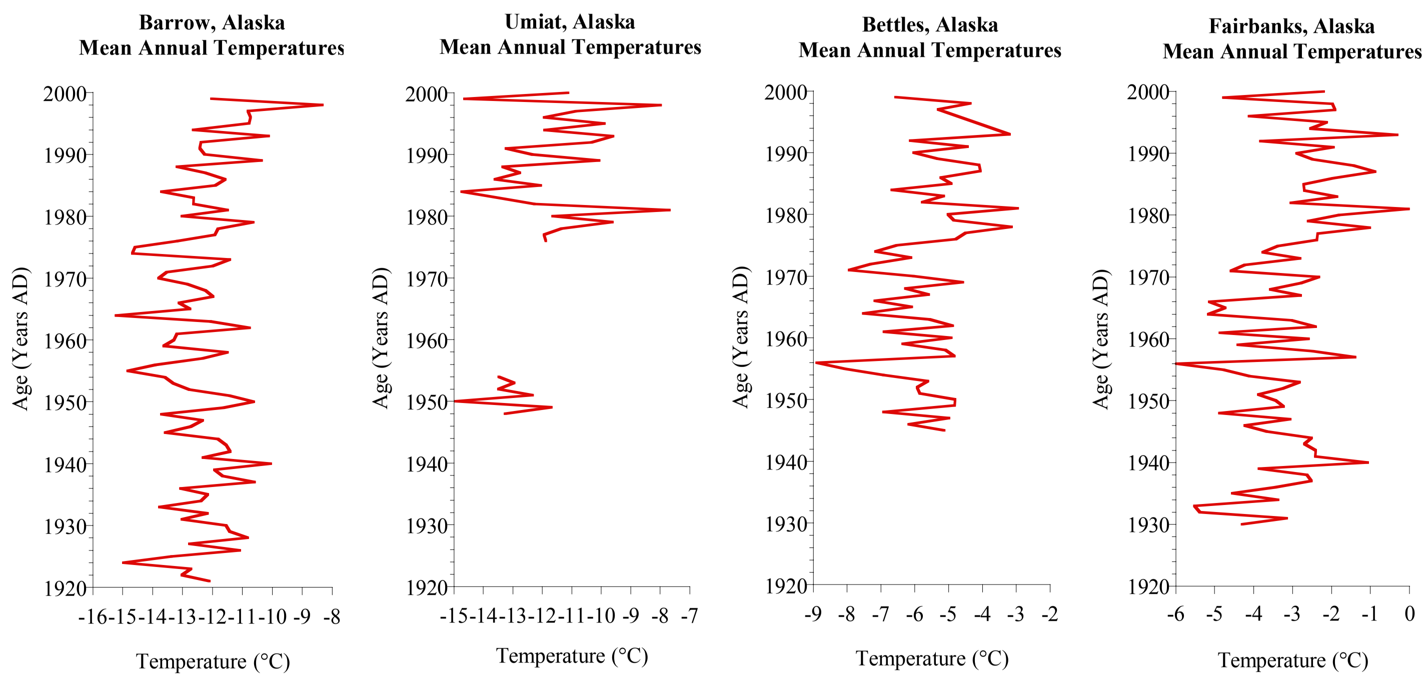

Figure 2.9: Mean annual temperature trends from instrumental data.

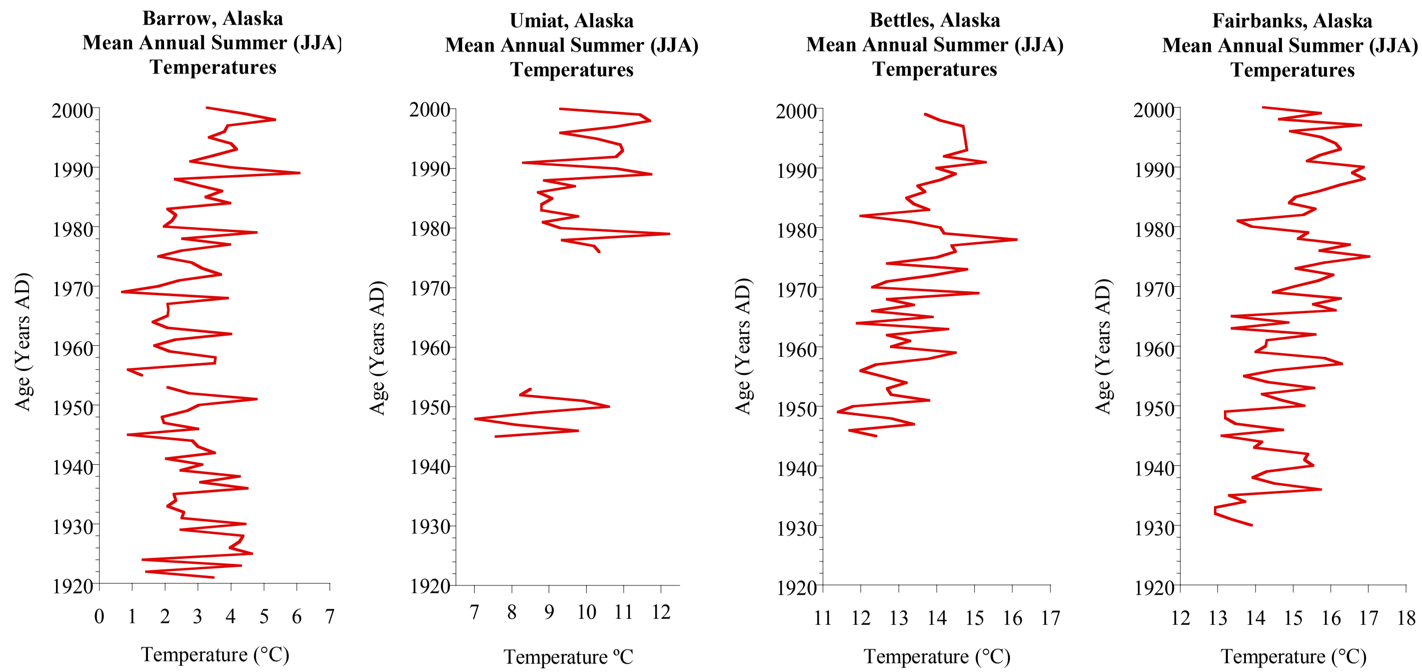

Figure 2.10: Mean summer (June, July, and August) temperatures.

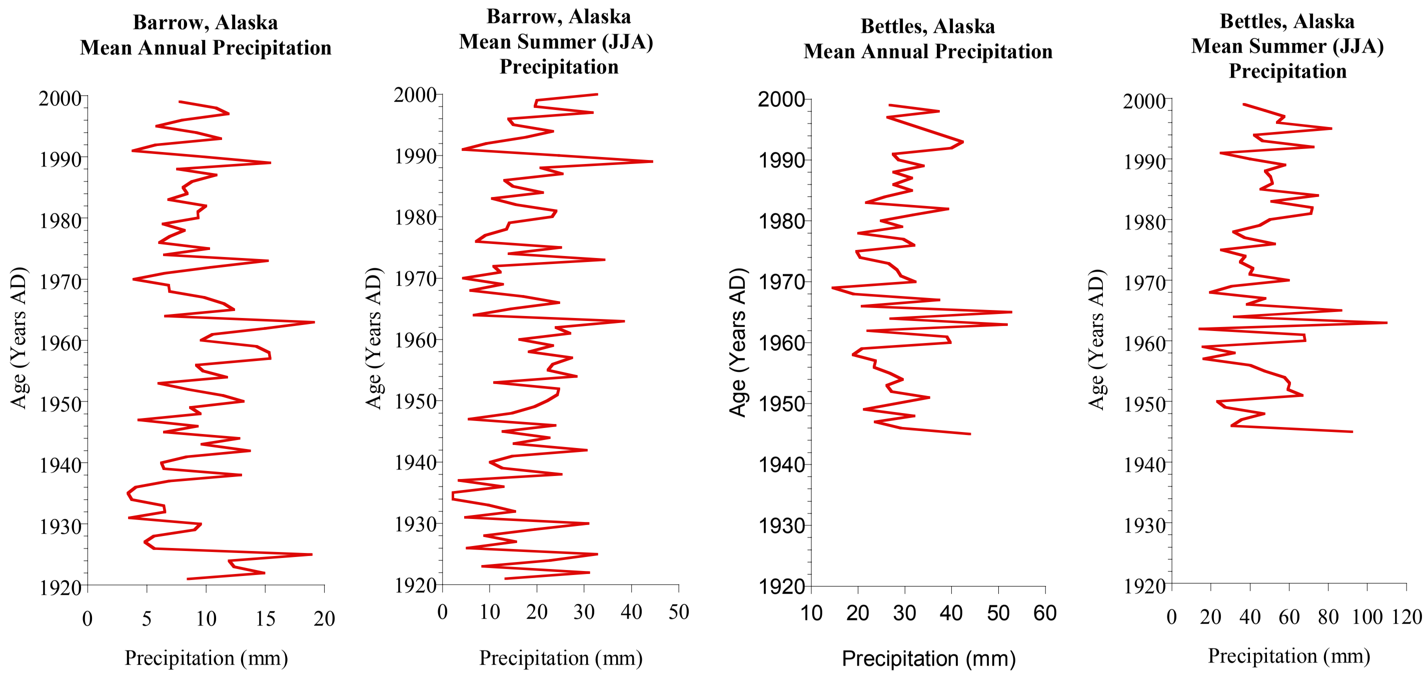

Figure 2.11: Average precipitation trends for Barrow and Bettles, Alaska.

Average precipitation at Barrow for the year 1993 AD was 19.09 mm. Other years of significant precipitation were 1989 AD (average = 15.38 mm), 1973 AD (average = 15.18 mm) and 1925 AD (average = 18.88 mm). Bettles had three significant years of precipitation in the 1960's – 1961 AD (average = 38.95 mm), 1963 (average = 51.69 mm) and 1965 (average = 52.63). Bettles did not have corresponding precipitation highs with Barrow during the years 1973 AD and 1989 AD

2.3 GLACIERS IN ALASKA

Glaciers cover approximately 74,700 km^2 (~5%) of the state of Alaska. Northward, the glaciers become smaller and more dispersed. In central and Arctic Alaska, the snowlines and glaciation thresholds occur between 1000 and 3000 meters rising eastward (Solomina and Calkin, 2003). The cirque glaciers of the Brooks Range are typically less than 2 km^2 in area and have north-facing orientations (Ellis and Calkin, 1979; Ellis and Calkin, 1984). Glacial geology studies show that radiation accounts for ~60% of ice and snow ablation of glaciers in the eastern Brooks Range (Wendler and Weller, 1974). Glacial response in the Brooks Range is of particular significance as a result of the combined effects of high latitude and distance from the main moisture source. Glacial geology studies show that under the present climate the cirque glaciers that dominate the North Slope of the Brooks Range in the Arctic, such as the one that feeds Blue Lake, are currently receding (Calkin et al., 1985; Ellis and Calkin, 1984). These glaciers are highly responsive to climate as is seen by the relatively large and easily induced mass balance fluctuations (Calkin et al., 1985).

3.0 MATERIALS AND METHODS

3.1 FIELD WORK

A sediment core was retrieved during the 1999 field season in August using a square-rod piston corer (Wright et al., 1984). The core was collected from the middle of the lake from a raft. Two 96 cm drives were obtained with a 20 cm overlap. Penetration of the sediment was unsuccessful after two drives. Retrieval of the uppermost sediments consisted of collecting a surface core adjacent to the original coring site. The surface core was sectioned in the field. The sediment core was transported unfrozen and stored at a constant 4ºC in cold storage facilities. The core was opened, cleaned and prepared for sub-sampling following procedures outlined in Lamoureux (1994) and Francus and Asikainen (2001).

The entire core was made into thin-sections and viewed using digital imaging techniques described in the methods section. Approximately two-thirds of the core was analyzed using petrographic microscopy and scanning electron microscopy with energy dispersive spectroscopy. The combination of the analytical techniques enabled detailed sedimentary and structural characterization to be constructed for the core.

A sub-sampling technique for preparing undisturbed thin-sections was used in order to preserve the structural detail of the sediment. This process involved shock freezing the wet, unconsolidated sediments, with liquid nitrogen, freeze-drying followed by vacuum impregnation using Spurr low-viscosity epoxy resin. High resolution image analysis was used to count and measure the thickness of the varves as per the methods outlined in Francus et al. (2002a). Sedimentary and mineral characterization was performed on a scanning electron microscope (SEM) coupled with energy dispersive spectroscopy (EDS). SEM permits high magnification analysis, quantified measurement, and characterization of sedimentary microsturctures (Krinsley, 1998).

3.2 THIN-SECTION PREPARATION

The preparation of undisturbed thin-sections is required to perform detailed analysis of varved sediments. Removing the interstitial water and embedding samples without disturbing the sediment structure is an involved process and can be done in several ways. The interstitial water must be removed first using either acetone replacement or freeze-drying (Lamoureux, 1994; Hughen et al., 1996; Francus and Asikainen, 2001). The method used here employed a freeze-drying technique and resin-impregnation using a low viscosity resin.

The sediment samples were extracted from split cores using sub-sampling boxes (Figure 3.1). The sub-sampling boxes were cut from aluminum sheeting and formed using a metal folding machine into 18 cm long x 1.5 cm wide x 0.7 cm deep rectangular boxes. Holes were punched along the bottom of the box to aid in epoxy penetration. The boxes were placed on the surface of the core and gently pushed by hand into the sediment. The boxes were positioned with a ~1 cm overlap sequence in order to sample the core continuously. A wire tool (Figure 3.2) was run beneath the aluminum boxes to separate the sediment from the core.

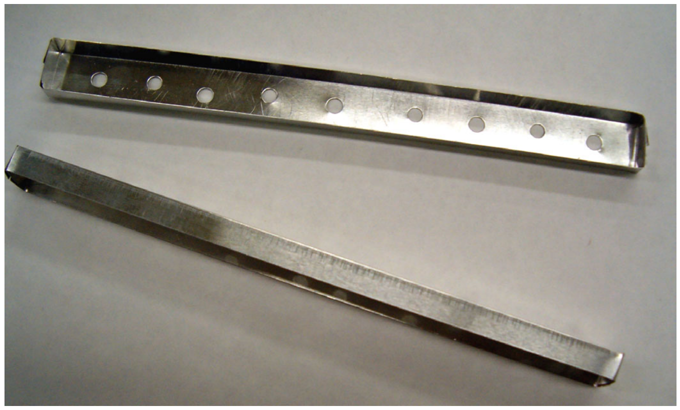

Figure 3.1: Aluminum sub-sampling boxes designed to cut out sediment from core.

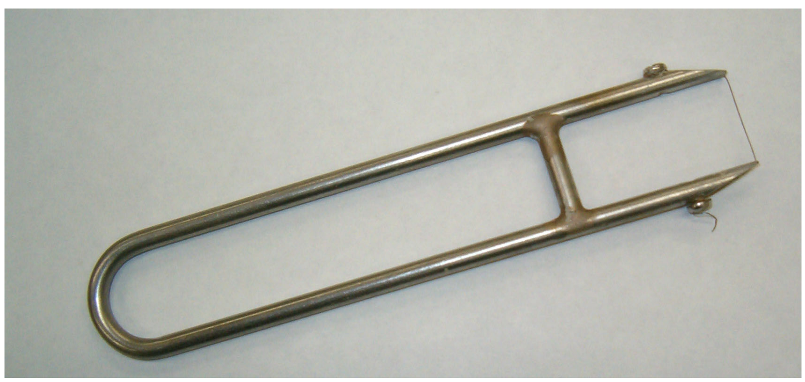

Figure 3.2: Tool used to remove sub-sampled sediment from core.

Freeze-drying the sub-samples utilized liquid nitrogen to freeze the water in the sediments without excessive ice-crystal growth. The sub-samples were placed in a small amount of liquid nitrogen (being careful not to submerse the entire sample) until frozen throughout. The frozen samples were immediately placed into the freeze-drier vacuum where the water was removed by sublimation. The samples were kept in the freeze-drier for 24 hours.

The samples were embedded with Spurr low-viscosity (20 cps) epoxy resin (Polysciences, 1992). Embedding was performed in disposable aluminum bread pans. These inexpensive containers were useful for all stages of the embedding process. Coarse plastic mesh (obtained at any local craft store) was placed in the bottom of the sample trays. The plastic mesh facilitated impregnation. Each container contained three labeled sub-samples. Spurr low-viscosity epoxy resin is prepared by mixing 4 components by volume. The resin can be mixed to provide a variety of hardness and curing times by varying the components. The mixture used was for a hardness suitable for thin-section grinding (Table 3.1).

Table 3.1: Proportions of epoxy components to be mixed in preparation of resin.

		x4	x8	x12
Vinylcyclohexene dioxide (VCD)	10g	40	80	120
Diglycidyl ether of Polypropyleneglycol (DER)	6g	24	48	72
Nonenyl succinic anhydride (NSA)	26g	104	208	312
Dimethylaminoethanol (DMAE)	0.4g	1.6	3.2	4.8

To ensure proper curing, the proportions were brought to weight dropwise using a pipette. The sub-samples were impregnated with epoxy under a light vacuum for 2 hours. Following impregnation, the sediment samples were cured for 48 hours in the oven at a temperature of 50ºC. Following curing, the 18 cm long impregnated slabs were separated using a rock (diamond) saw and cut into three 7 cm long sections with a 45º angle to the bedding to insure an entire sedimentary succession. The samples were sent to a commercial preparation facility for final thin-sectioning

The fine-grained, clay-rich composition made embedding the sediments with epoxy resin a challenging process. The embedding process was most efficient in the section of the core that contained thinnest varve couplets. Difficulties were encountered when impregnating the sections of the core with the large, anomalously thick units. These consisted of large (>1 cm) layers of (graded) very fine-grained clays. The center of these large units often did not embed well. However, enough of the surrounding outside was embedded to make the proportions of the unit identifiable. This problem was most significant near the top and in the bottom portion of the core where changes in sedimentation to Blue Lake resulted in the deposition of many of the larger lamina.

3.3 VARVE ANALYSES

As of yet, there is no reliable automated varve counting system available. However, a computer algorithm has been developed to aid in manual counts (Francus et al., 2002a). The algorithm, written in Visual Basic, works with Adobe Photoshop and Microsoft Excel. The source code is available at http://www.geo.umass.edu/climate/soft/soft.html. First, the thin-sections were digitized at 1440 dpi using a flat bed scanner with transparency capabilities (Figure 3.3). Adobe Photoshop was used because its *Path* function exports files in a PostScript format. In the *Paths* layer of Adobe Photoshop, the boundaries of each lamination were marked by drawing straight, horizontal lines using the *Pen Tool*. A straight vertical line was drawn perpendicular to the horizontal lamination boundary lines. Next, the path was exported using the *Paths to Illustrator* feature. The exported files are PostScript files and contain information that includes the coordinates of the lines. The laminations need to be horizontal and some adjusting of the image was necessary using the *Rotate Canvas Arbitrary* tool. To avoid measuring cracks or other disturbances in the thin section as part of a lamination, a new vertical line was started where the disturbance occurs. The algorithm utility automatically computed the offset.

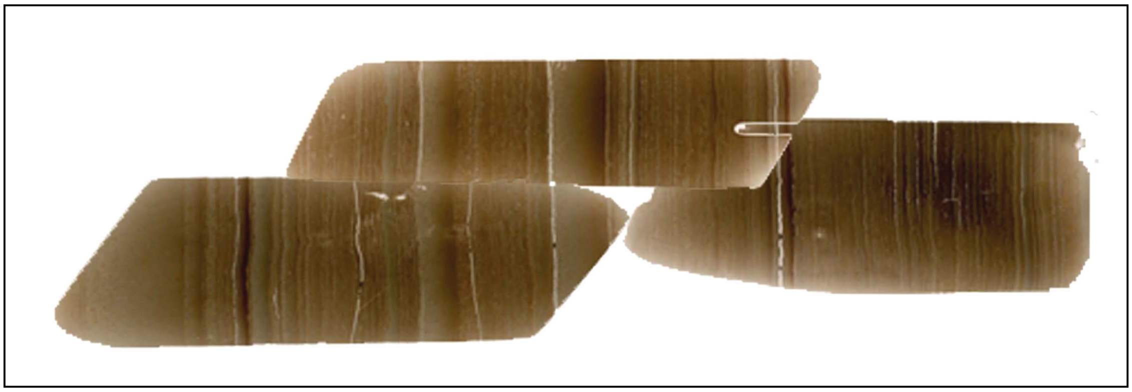

Figure 3.3: Digital image of scanned thin-sections from Blue Lake sediment core.

The algorithm utility was saved as a Microsoft Excel macro and opened each of the exported files as text files. The resulting output Excel file contained the depth coordinates in centimeters of each lamination boundary that was manually marked on the image and included the number of boundaries. The depth coordinates were converted into thickness values in centimeters. The dark (winter) lamina were used as the varve boundary.

High-resolution imaging techniques provided several advantages over other methods studied such as improved efficiency and speed of the counting process and it relieved some of the tedious manual labor involved in the construction of a varve chronology. More importantly it has provided digital documentation and storage of the Blue Lake varve chronology. This allowed for easy review or revision of the chronology and permitted a straightforward comparison of multiple counts. Scanning at a 1440 dpi resolution set the pixel size at 17 μm. This permitted varves as thin as 300 μm to be measured with an accuracy of 6%. The *Path* function of Adobe Photoshop was much more flexible and had several advantages over other freeware image analysis programs. First, the multiple counts required could be performed on the same background thin-section image. The *Paths* could be hidden allowing for the additional counts to be made without the influence of previous counts (Francus et al., 2002a). Analysis of digital thin-sections provided a mechanism for a quick and easy way to zoom in and out in order to view both a large-scale overview and a high-resolution close-up of the sedimentary fabric when needed.

Sedimentary and mineral characterization was performed on a scanning electron microscope (SEM) coupled with energy dispersive spectroscopy (EDS). A SEM equipped with an EDS is used routinely in mineralogy and is considered an accurate tool for investigating the elemental concentrations within sediment laminations (Saarnisto, 1986). SEM permits high magnification examination of individual mineral grains, pore spaces, evidence of bioturbation and sedimentary fabric. The SEM provides quantified measurements and characterization of sedimentary microstructures, such as packing, grain-size, shape and composition (Krinsley et al., 1998). SEM scans the surface of a specimen with a focused electron beam. The beam-specimen interaction generates a variety of signals that may be collected and displayed in different modes (Figure 3.4).

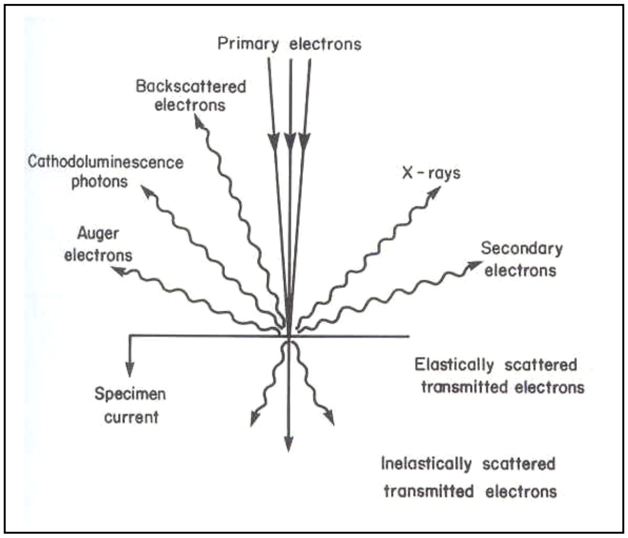

Figure 3.4: Signals generated by beam-specimen interaction during SEM (Krinsley et al., 1998).

The three most common signals used are backscattered electrons, secondary electrons, and x-rays. In the backscattered electron (BSE) mode, the image is based on compositional contrast. Backscattered electron imaging provides visual information based on gray-scale intensity or contrast between chemical phases. Backscattered electrons are high-energy electrons that are reflected from the specimen surface. The quantity of electrons backscattered correlates to the atomic number; an element with a high atomic number will produce more backscattered electrons than an element with a low atomic number. This generates a contrast between different phases that can easily be distinguished in the backscattered electron image.

Varve thickness time series were first standardized using a simple dendrochronological index (Fritts, 1976). The index is calculated as follows:

$$x_i = \frac{x_o}{x_e}$$

where x_i is the index value, x_o is the observed lamination thickness and x_e was the expected value derived from a linear function of the thickness series. Index values were then standardized to a "zero mean":

$$Z_n = \frac{i - \mu}{s}$$

where Z_n is the standardized varve thickness value (normalized), i is the index value, μ is the arithmetic mean of all analyzed varve thickness values, and s is the standard deviation of the series.

3.4 RADIOMETRIC DATING

Independent dating techniques were used to verify varve chronology of Blue Lake. Samples were analyzed at the Freshwater Institute in Winnipeg, Manitoba. A surface core was retrieved and sampled in the field and submitted for analysis for ^{210}Pb and ^{137}Cs. In addition, the Blue Lake core was sampled in the laboratory at 0.5 cm intervals (0.5 cm x 0.5 cm x 1 cm) up to a depth of 10 cm for ^{137}Cs analysis.

4. 0 RESULTS

4.1 SEDIMENTOLOGY

The varves in Blue Lake are rich in allochthonous mineral matter with very low concentrations of organic matter (<2%). Varve couplets representing one year are characterized by a layer of thick, light colored, clay to silt-sized material (spring-summer) overlain by a thinner, dark colored, fine-clay cap (winter) (Figure 4.1). The spring/summer layers contain abundant grains of quartz and feldspar with lesser amounts of clay while the winter layer consists entirely of extremely fine-grained clays.

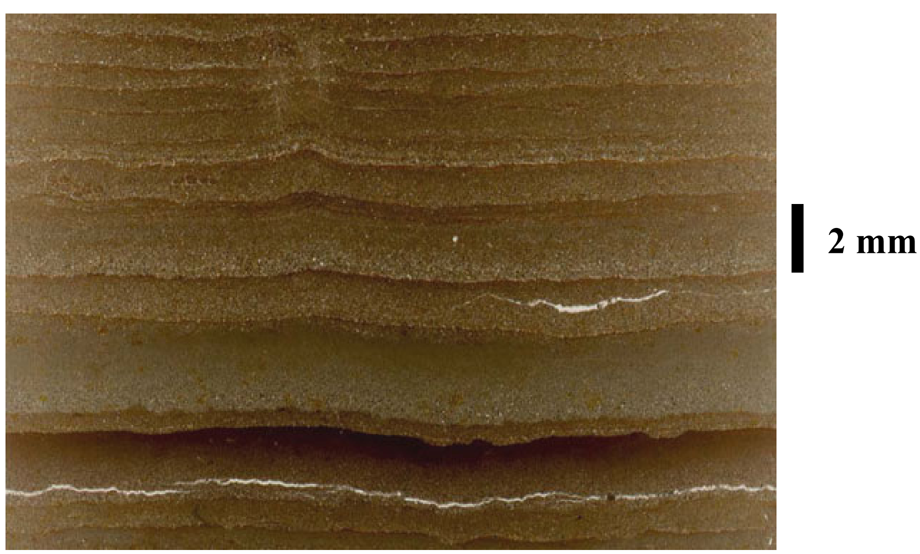

Figure 4.1: Scanned image of Blue Lake varves showing typical laminated sediments.

Backscattered electron (BSE) images with energy dispersive spectroscopy (EDS) (Figure 4.2a and b) illustrate the size, shape, and elemental composition of the sediment. Figure 4.2a represents a typical coarse-grained spring layer. The morphology and elemental spectrum are consistent with alumino-silicate mineral matter, such as quartz, feldspars (potassium), and clays rich in magnesium and iron. The major elements present are aluminum and silicon with minor amounts of potassium and magnesium. Trace amounts of particles rich in iron, titanium (possibly rutile), phosphorus/calcium (possibly apatite), and barium/sulfur were also observed. The coarse sediment layers are composed of coarse grains that range in size from approximately 10 to 100 μm. The quantity of minerals, such as quartz and feldspar, decreases and the size becomes smaller as layers become finer. The winter clay cap marks a noticeable decrease in grain-size (Figure 4.2b) and is homogeneously composed of fine-grained clay minerals. The clay minerals present in the winter clay cap are exclusively <10 μm in size. This was consistent for all layers identified throughout the core. The transition from the spring course-layer to the fine-grained winter clay cap is often a graded, fining-upward sequence. However, the transition between the winter clay-layer and the next spring melt-layer is generally abrupt. This is consistent with the influx of large quantities of terrigenous material as a result of glacier runoff caused by warming temperatures (Hardy, 1996). As the season progresses, available energy of transport decreases and the grain-size transported to the lake becomes smaller resulting in the fining-upward sequence. Based on their internal structure, composition, and depositional setting, the laminated sediments in Blue Lake are consistent with varves formed in glaciolacustrine environments and are true bimodal clastic varves (Sturm, 1979; O'Sullivan, 1983).

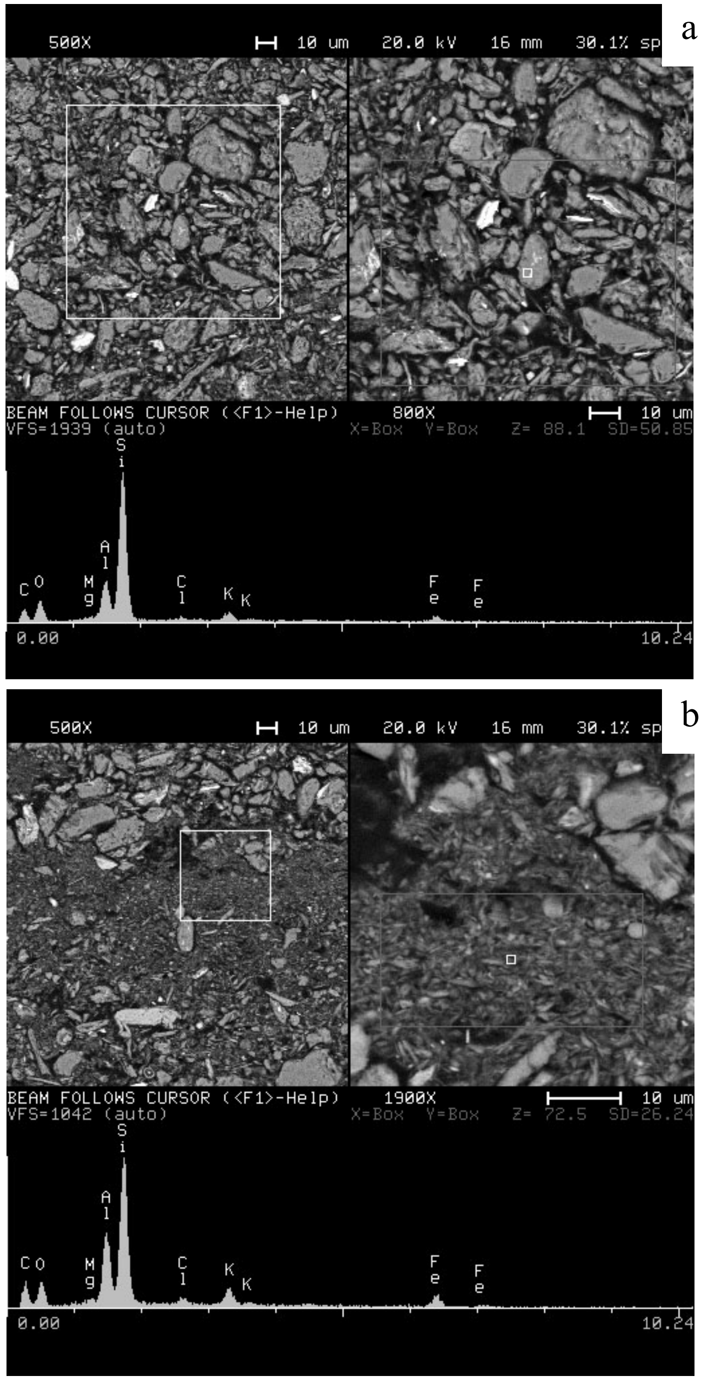

Figure 4.2: SEM-BSE images and elemental spectra of (a) coarse spring/summer lamina and (b) fine-grained winter clay cap. Elemental chlorine observed throughout the EDS analysis is derived from the epoxy resin.

Anomalously thick sedimentary units (>1 cm) consisting of a fining upward sequence (Figure 4.3) were observed primarily in the top 25 cm and the bottom 60 cm of the sediment core. Less frequently observed in the Blue Lake core were massive structures (>2 cm) with unique sedimentary features (Figure 4.4) observed in the upper 25 cm and lower 40 cm of the core. These large structures exhibit a relatively coarse base and grading (fining upward sequence) and contain massive amounts of very fine-grained clays. The structure shown in figure 4.4 is exceptionally large and was observed from 6 – 10 cm in core depth.

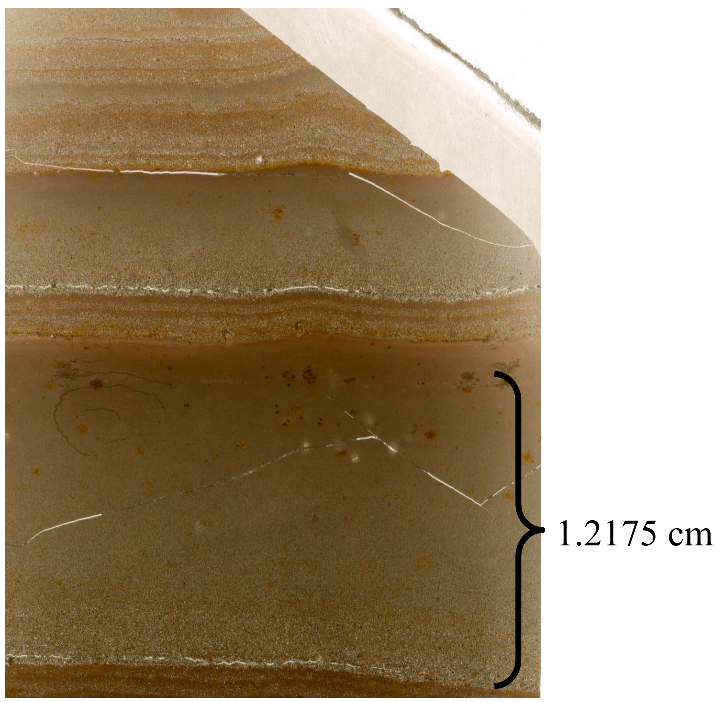

Figure 4.3: Image of a scanned thin-section illustrating an anomalous thick sedimentary unit observed primarily in the upper and lower portions of the core.

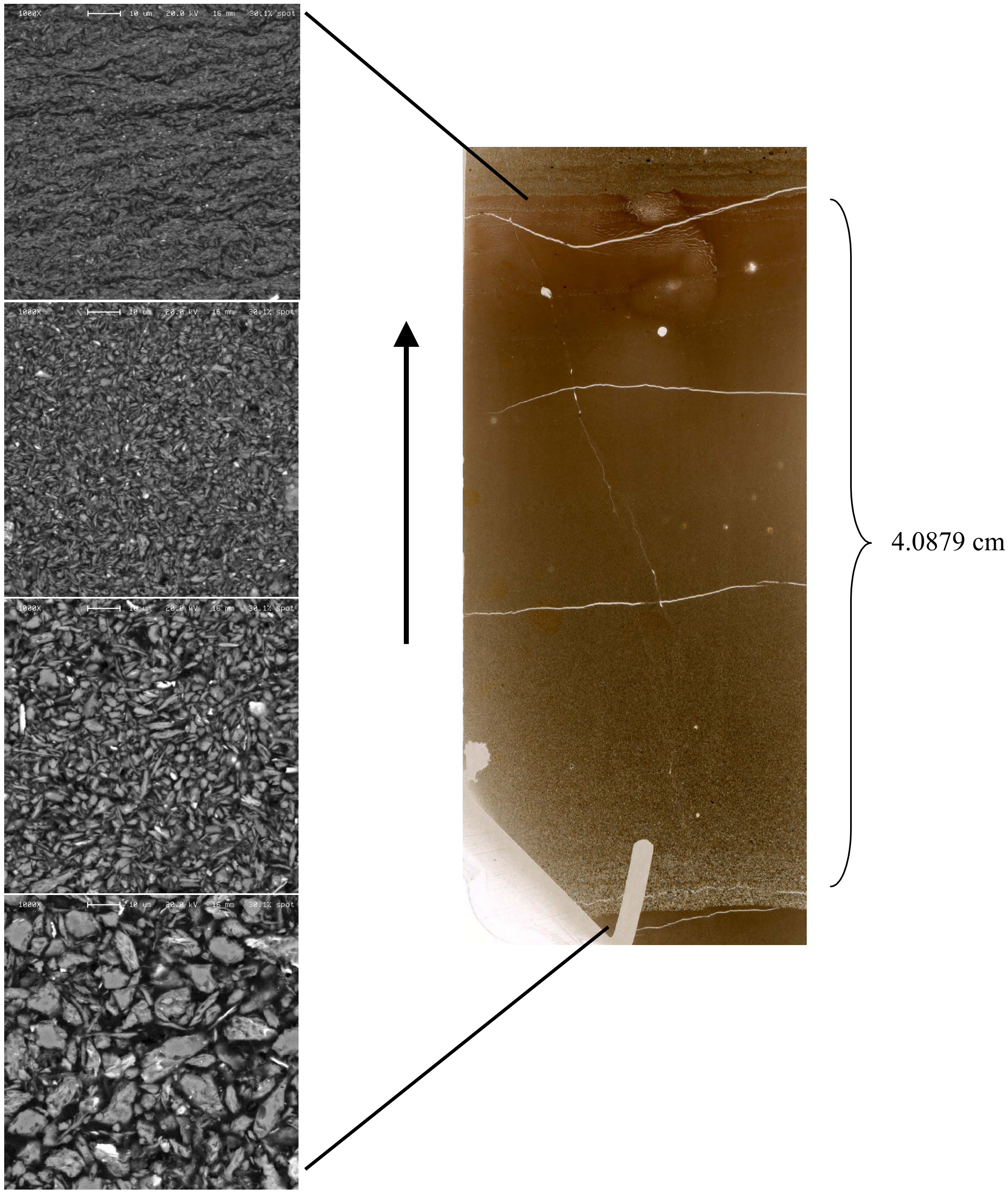

Figure 4.4: BSE images (at 1000x) and scanned thin-section illustrating one of the massive sedimentary structures observed primarily in the top portion of the core.

4.2 BLUE LAKE RADIOMETRIC DATES

^{137}Cs analysis of the surface core identified a peak in ^{137}Cs activity at a depth of 5.25 cm (Figure 4.5). Inconsistencies in the ^{210}Pb activity downcore prevented the use of the CRS or CIC dating models. The high and variable sedimentation rate to the lake coupled with the low flux of radionuclides at high latitudes may have complicated the use of the ^{210}Pb dating techniques. However, despite the difficulties encountered in developing a radiometric-based chronology using the surface core, a ^{137}Cs chronology was established using the sectioned Blue Lake core. The ^{137}Cs peak was identified at a depth of 3.75 cm (Figure 4.5). A smaller peak in ^{137}Cs activity was identified at a depth of 2.75 cm. According to Stihler et al. (1992), the peaks of ^{137}Cs fallout exist in the sediment record corresponding to 1963 AD and 1986 AD. Atmospheric fallout from nuclear weapons testing reached a maximum in 1963 AD creating a distinct peak of ^{137}Cs-activity. Atmospheric ^{137}Cs has been negligible since the 1980's. However another smaller peak could be the result of the Chernobyl disaster in 1986 AD.

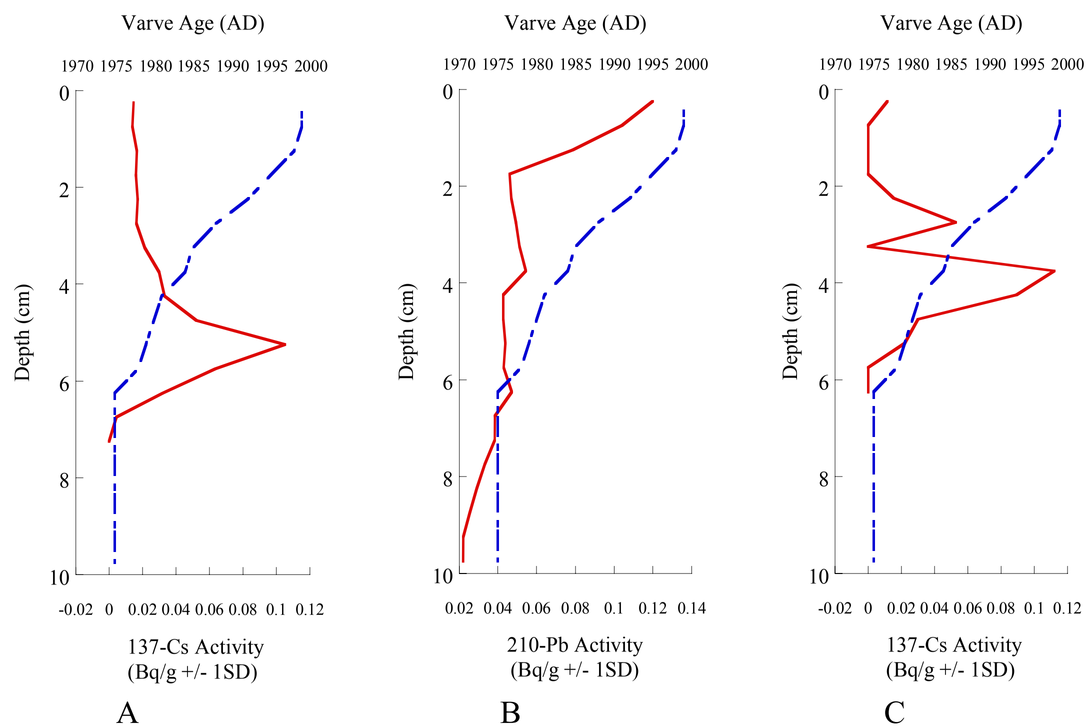

Figure 4.5: ^{137}Cs and ^{210}Pb activity from the surface core (A and B) and sectioned Blue Lake core (C).

4.3 BLUE LAKE VARVE SERIES

Two chronologies will be presented and discussed in this study because of the problems encountered with radiometric data. The first chronology presented is the raw measurements without manipulation as they were counted with the first true varve at the top of the core representing the full year before core collection (1998). The second chronology has been adjusted to the ^{137}Cs results measured from the Blue Lake core. The two chronologies differ by 21 years. However, the overall broad trends are not changed.

4.3.1 Original Varve Chronology

A plot of the raw varve thickness measurements and the standardized counts from Blue Lake is shown in Figure 4.6 and 4.7 and descriptive statistics are presented in Table 4.1. The varve thickness measurement results show variable sedimentation rates throughout the record. The varve record spans the calendar years from 922 AD to 1998 AD. Varves are relatively thick from the period 922 AD to approximately 1030 AD. Overall, varve thickness gradually declines with occasional interruption containing slightly thicker layers (for example, 1100 AD to 1160 AD, 1340 AD to 1360 AD, and 1540 AD to 1600 AD). A period of relatively stable, low sedimentation formed the thinnest laminations of the record during the period from 1600 to 1900 AD. Varve thickness abruptly increases after 1900 AD.

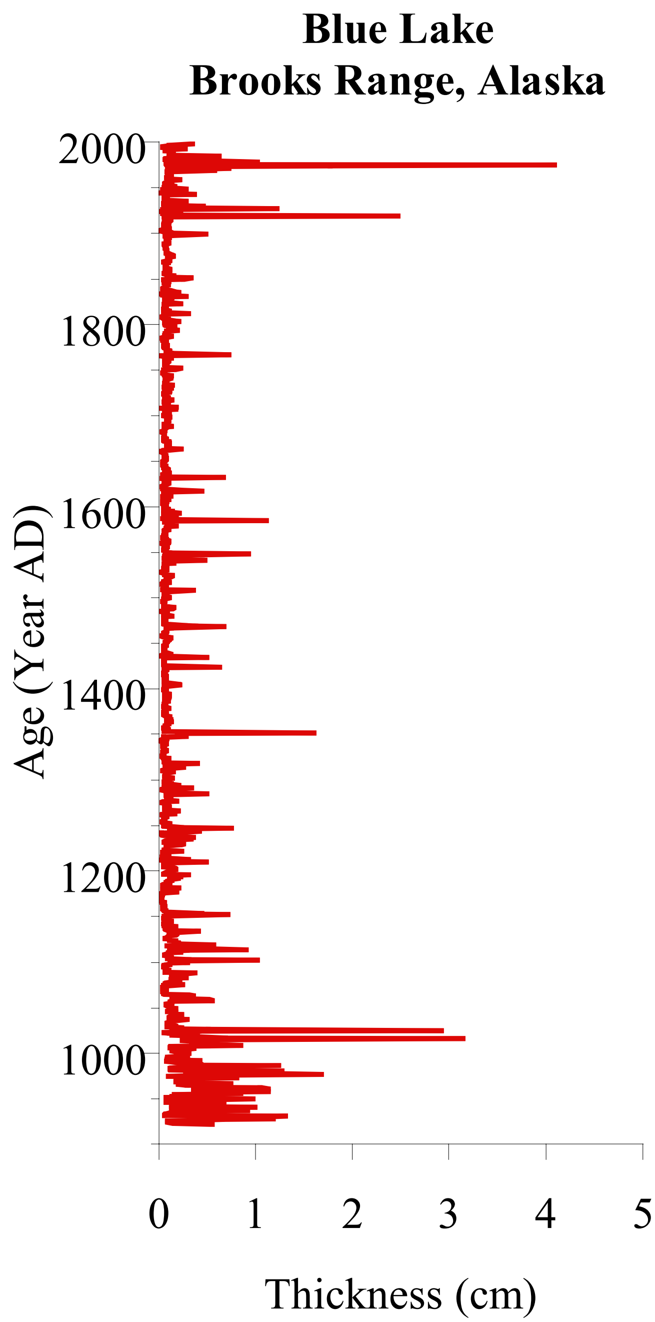

Figure 4.6: Raw varve thickness measurements for Blue Lake core.

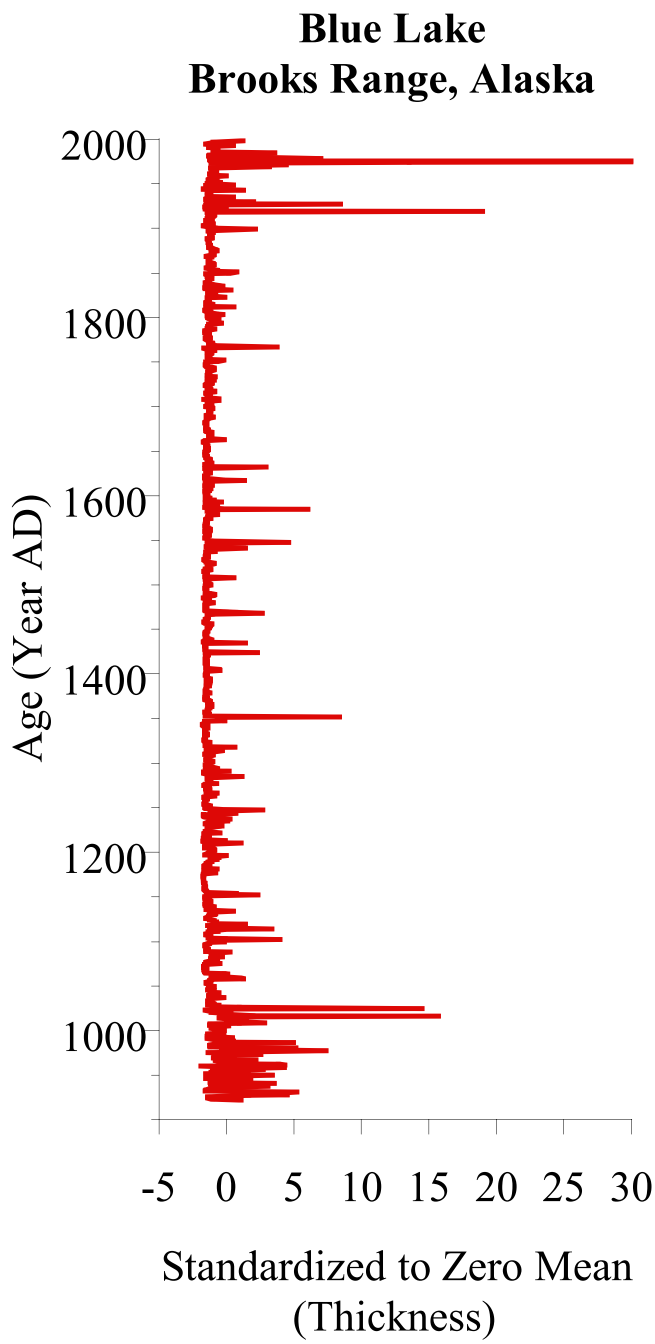

Figure 4.7: Standardized to zero mean varve thickness for Blue Lake core.

Table 4.1: Descriptive statistics for Blue Lake varve series.

Mean	Variance	Std. Dev.	Skewness	Kurtosis
0.15	.072	0.27	7.29	76.16

4.3.2 Cesium Adjusted Chronology

The ^{137}Cs peak indicting the year 1963 AD to 1964 AD was identified at a depth of 3.75 cm in the Blue Lake core. Setting the varve observed at 3.75 cm to the year 1963 AD shifts the chronology down 21 years (Figure 4.8). The adjusted varve record spans the calendar years from 901 to 1977 AD.

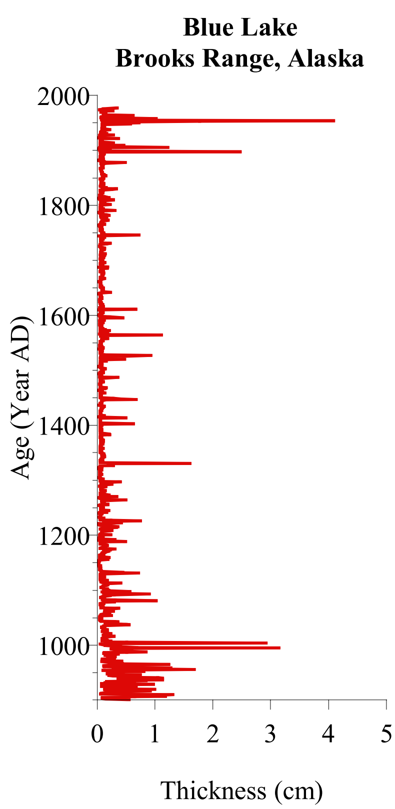

Figure 4.8: Raw varve thickness measurements for Blue Lake core adjusted for ^{137}Cs results.

5.0 DISCUSSION

5.1 METEOROLOGICAL DATA

The hypothesis that variations in varve thickness reflects changes in summer air temperature was tested by comparing the Blue lake varve thickness record with meteorological data from the surrounding weather stations at Barrow, Bettles, Fairbanks, and Umiat (refer to figure 2.6 for locations of meteorological stations used in this study). Differences in elevation, aspect, and surrounding topography result in considerable variability among weather stations making the correlation between varve thickness data and station measurements difficult (refer to section 2.2). Mean annual and mean summer (JJA) temperatures from four of the meteorological stations were compared to determine if there is a relationship between historical climate data and varve thickness at Blue lake (Tables 5.1 and 5.2).

Table 5.1: Comparison of mean annual temperatures for Alaskan meteorological stations.

Meteorological Stations	Barrow vs. Umiat	Barrow vs. Bettles	Barrow vs. Fairbanks	Bettles vs. Umiat	Bettles vs. Fairbanks	Fairbanks vs. Umiat
r-squared	0.287	0.40	0.25	<0.01	0.77	0.08
Correlation Coefficient	0.54	0.63	0.50	-0.03	0.88	-0.29

Table 5.2: Correlation of mean summer (JJA) temperatures for meteorological stations.

Meteorological Stations	Barrow vs. Umiat	Barrow vs. Bettles	Barrow vs. Fairbanks	Bettles vs. Umiat	Bettles vs. Fairbanks	Fairbanks vs. Umiat
r-squared	0.54	0.07	0.17	<0.01	0.02	0.13
Correlation Coefficient	0.74	0.27	0.42	0.05	0.41	0.36

The strongest correlation between metrological measurements and varve thickness at Blue Lake is with station data from Bettles and Fairbanks, both located within the Interior climate zone of Alaska. Barrow and Umiat, located within the Arctic climate zone, agree relatively well with each other, but not with the Blue Lake varve thickness record. Data from Bettles correlated poorly with Umiat (r = -0.02 and r = 0.05 for mean annual temperature and mean summer temperature, respectively). The relatively weak correlation between Umiat and several of the other stations may be a result of the location (different climate zones), short duration of data, or decreased accuracy because Umiat is not a first order weather station.

The Blue Lake varve thickness data correlated best with the meteorological data from Fairbanks, both show a warming in the 1970's (Figure 5.1). However, there are limitations to this comparison because of the distance and geographic differences between the sites.

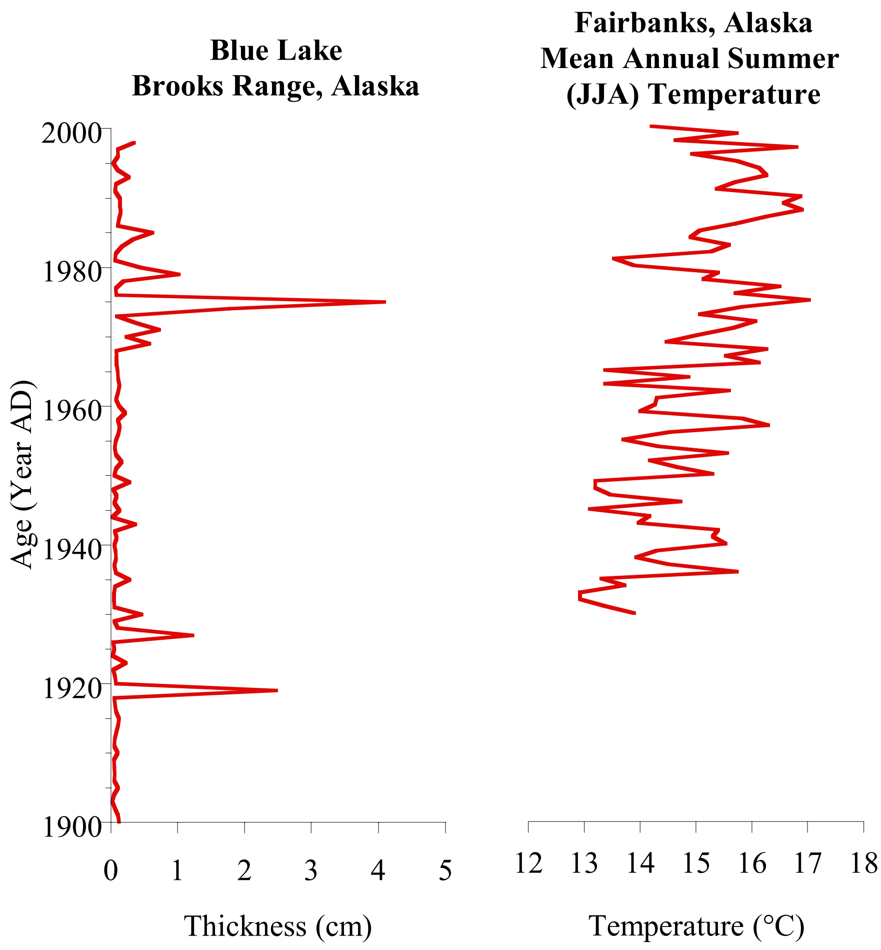

Figure 5.1: Unadjusted varve chronology compared to Fairbanks instrumental data.

5.2 NORTHERN HEMISPHERE TEMPERATURE RECONSTRUCTION

5.2.1 Medieval Warm Period

A relatively warm period from ~1000 AD to 1400 AD, referred to as the Medieval Warm Period (MWP), was observed in western Europe, Greenland, and Arctic Canada (Lamb, 1995). Some historical records place the MWP as early as 800 AD with dates varying by 200 years. For example, coastal Greenland began experiencing the MWP as early as 800 AD, approximately 100 years earlier than in Europe (Meese et al., 1994). In the High Arctic, the existence of a similar warm, yet variable, period is supported by paleoclimate proxy evidence. Thick varve measurements during the early part of the Blue Lake record between 900 AD and 1300 AD correspond well to the timing of the MWP, suggesting warm conditions existed in the interior and Arctic regions of Alaska.

5.2.2 Little Ice Age

The Little Ice Age (LIA) was a period associated with widespread glaciation and cooler temperatures. The LIA has been identified at many locations throughout the Northern Hemisphere, however the timing of its onset and demise vary from region to region (Bradley and Jones, 1993; Overpeck et al., 1997; Mann et al., 1998). Overpeck et al. (1997) reported that the LIA in the Arctic began sometime before 1600 AD and ended in the mid-19th century. Other studies in Europe suggest dates ranging from 1200 AD to 1800 AD and from 1350 AD to 1900 AD (Meese et al., 1994; Lamb, 1995). The timing of the onset of the LIA corresponds with: (1) the time that the Thule changed their diet from whale to seal as a result of increased sea ice, (2) the abandonment of the western Norse settlement in Greenland at ~1350 AD (McGovern, 1991; Barlow et al., 1997), (3) glacial advances in the Brooks Range (Ellis and Calkin, 1984), and (4) paleotemperature reconstructions showing cold conditions in Greenland based on ice core studies (Fischer et al., 1998). Blue Lake varve thickness gradually declines between 1300 AD and 1600 AD to the thinnest couplets formed during the >1000-year record, suggesting cold conditions between 1600 AD and 1900 AD. This corresponds well with LIA in the Northern Hemisphere.

5.2.3 Twentieth Century Climate

While most records suggest an unprecedented 20th century warming, there is variability from region to region in the timing of its onset and magnitude (Lamoureux et al., 2004). Several studies suggest that the Arctic has experienced warming during the period from 1845 AD to 1950 AD (Fisher, 1977; Jacoby and D'Arrigo, 1989; Bradley, 1990; Lamoureux and Bradley, 1996). Lamoureux and Bradley (1996) documented the period from 1931 AD to 1960 AD as having been 80% warmer in the Arctic than the prior 3000 years. The dramatic increase in varve thickness around 1900 AD in the Blue Lake record corresponds to the 20th century warming trend. The northern hemisphere multiproxy temperature reconstruction published by Mann and Jones (2003) shows the MWP, LIA, and 20th century warming and compares well with the Blue Lake varve thickness record interpreted as a record of summer warmth (Figure 5.2).

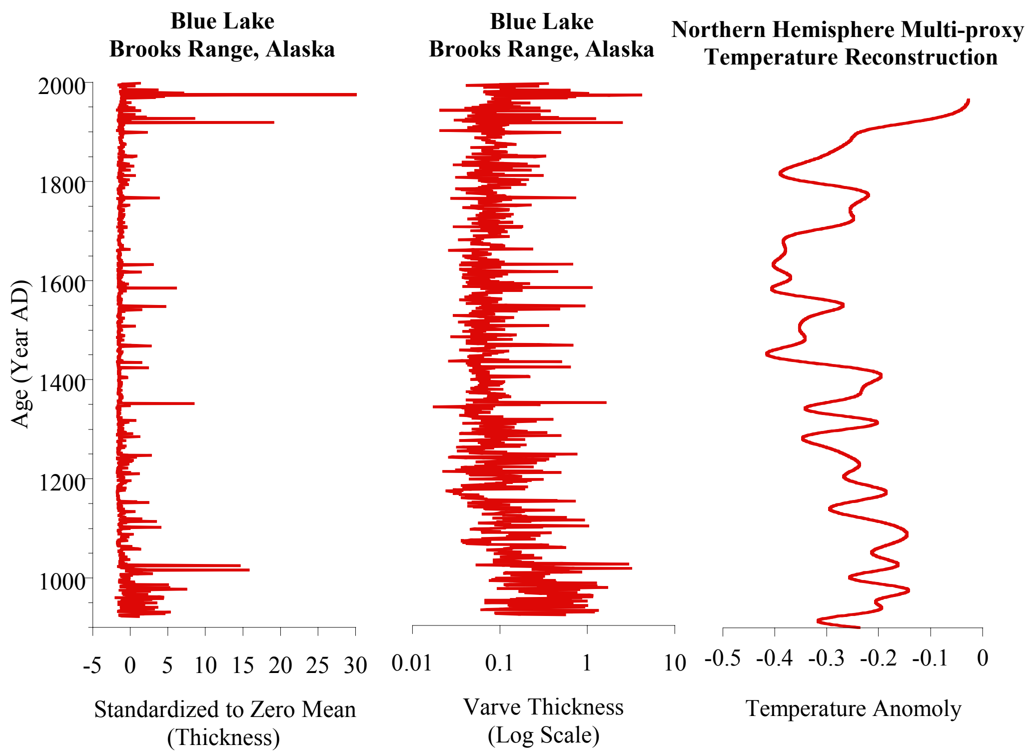

Figure 5.2: The northern hemisphere multiproxy temperature reconstruction published by Mann and Jones (2003) showing the MWP, LIA, and 20th century warming compared to Blue Lake varve thickness record.

5.3 BROOKS RANGE GLACIAL CHRONOLOGY

Warming and cooling trends suggested by the Blue Lake varve record compare well with the late-Holocene glacial history of the Brooks Range as determined from glacial geology studies (Calkin et al., 1985; Ellis and Calkin, 1984). Glacial moraine records from the Brooks Range dated by lichenometry and radiocarbon measurements indicate several glacial advances and retreats during the late Holocene. One of these advances, dated by lichenometry, is believed to have occurred 390 ± 90 years BP (before present). By convention "present" is set at 1950 AD as this is the time when radiocarbon dating was first used, so 390 BP is 1460 AD. Ice margins likely remained close to this position until around 1640 AD to 1750 AD when glacial retreat began (Ellis and Calkin, 1984). Studies of the cirque glaciers that are present on the northern slope of the Brooks Range indicate that the glaciers are currently receding and that retreat has increased significantly since the 1950's (Calkin et al., 1985; Ellis and Calkin, 1984). Comparison of air photos of the Blue Lake watershed taken in 1970 AD and 1979 AD show that the glacier above Blue Lake has receded during this period, supporting these observations. The retreat of the glacier is recorded in the varved record of Blue Lake by thick laminations since ~1970 AD. In addition, instrumental records show increased temperatures since ~1970 AD. Global-scale glacial retreat has been observed since the middle of the 19th century and continued at increasing rates during the late 20th century. Regions of glaciation in the Northern Hemisphere have seen a shift to warmer and more humid conditions, particularly since around 1977 AD, with both winter accumulation and summer melting increasing (Dyurgerov et al., 2000).

5.4 CIRCUM-ARCTIC COMPARISON

A variety of paleoenvironmental records spanning the last millennium have been established across the Arctic and are used here for comparison with the Blue lake varve thickness record (Figure 5.3). These paleoclimate records include cores of glacial ice, lake sediment records, and tree-ring studies. Ice cores provide information for past environmental conditions, such as net accumulation, percent melt, temperature inferred from stable isotope ratios ($\delta^{18}O$), and atmospheric composition from trapped gas in the air bubbles contained within the ice core providing a record of past levels of CO_2, CH_4, and NO_2 (Thompson, 1989). $\delta^{18}O$ measurements in the ice cores can be interpreted as an indicator of temperature (Jouzel et al., 1983). Additionally, melt layer frequency has been used to infer summer melting and provides a proxy for comparison with varve thicknesses. The relationship between the stratigraphy of the ice and climate change can be inferred from a statistical analysis of melt features within the ice core. Summer meltwater in the firn zone of a subpolar ice cap seeps through the firn and snow and refreezes to form distinct stratigraphic features (Koerner, 1977; Koerner and Fisher, 1990). Studies that look to establish summer temperatures as proxies of summer ablation typically use melt percent records (Koerner and Lundgaard, 1995). Ice cores retrieved from ice caps, such as those in the Canadian Arctic Archipelago, can provide paleoclimate information on an annual, decadal, centennial, or millennial scale of resolution depending on the proxy of interest (Bourgeois et al., 2000). Varved lake records from Ellesmere Island, Baffin Island, and Devon Island are additional high-resolution paleoenvironmental records for comparison (Lamoureux et al., 2004; Smith et al., 2004).

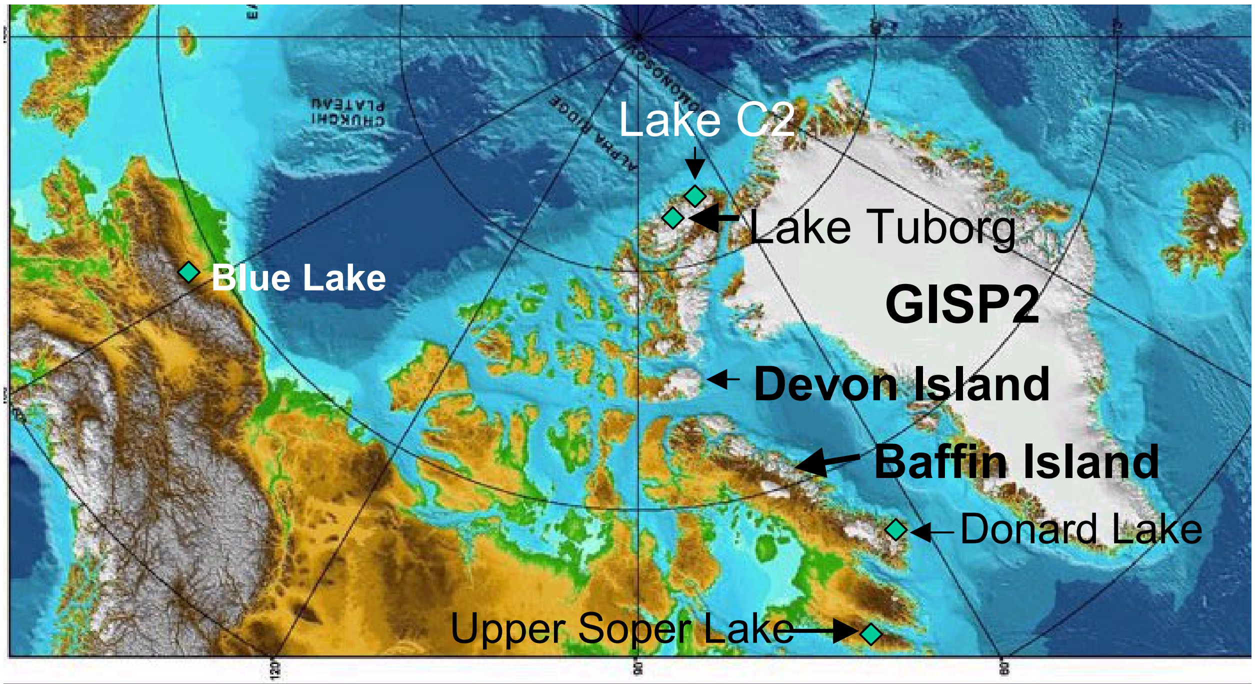

Figure 5.3: Location of paleoenvironmental records from the Arctic region used in this study.

5.4.1 Ice Core Records

Ice core results indicate that during the timing of the LIA, the Devon (Fisher, 1977) and Agassiz Ice Caps (Koerner and Fisher, 1990) recorded a cold interval (Figure 5.4). A closer look at the Devon Ice Cap melt record shows a period of colder summers between about 1600 AD and 1925 AD. This cold period corresponds to the time when the thinnest laminations were formed in Blue Lake. The ice core profiles indicate a large increase in melting beginning in the middle 1920's. In the Devon Ice Cap melt record, post-1920's melting rose to a peak in the 1930's, diminished during the 1940's, and increased again in the 1950's and 1960's. A comparison of melt percentages in ice cores from the other major Canadian Arctic ice caps suggests that past summer conditions identified from the Devon Island ice cap are representative of the large ice caps 90% of the time (Koerner, 1977). The composite ice core melt records retrieved from the Devon and Agassiz Ice Caps indicate that the past 100 years has had the warmest summers of the past 1000 years (Koerner and Fisher, 1990; Koerner, 1977). Holocene $\delta^{18}O$ profiles also showed increased warmth during the 20th century (Figure 5.5) (Bourgeois et al., 2000). Both summer melt and $\delta^{18}O$ values have increased this century, the timing of which correspond to a period of thick varves in the Blue Lake record. This similarity suggests that the Brooks Range may have undergone significant warming during the past 100 years. This warming, expressed in the Blue Lake record, abruptly increase in both frequency and magnitude following the 1900's.

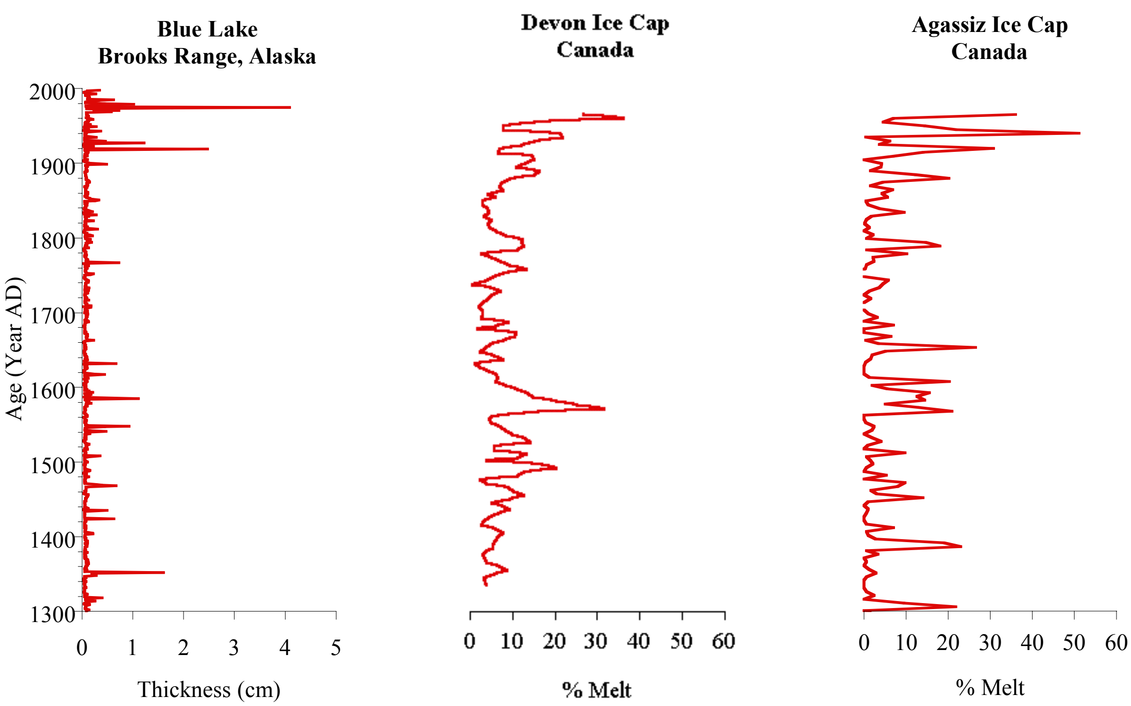

Figure 5.4: Comparison of the unadjusted Blue Lake varve thickness measurements with the Devon and Agassiz Ice Cap melt records.

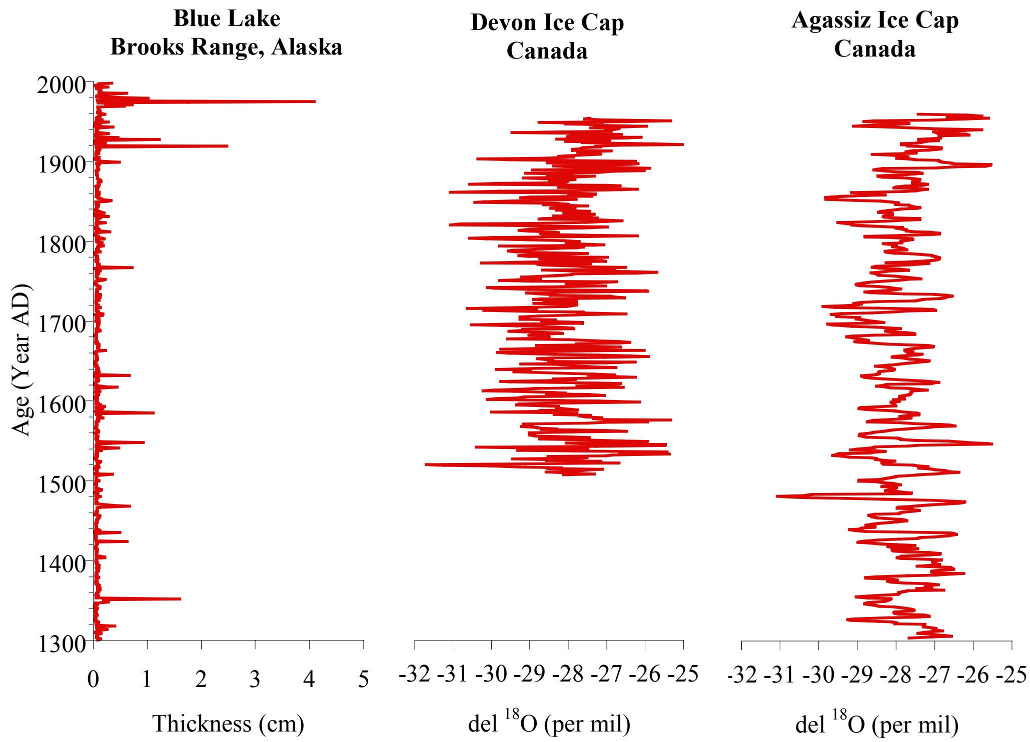

Figure 5.5: Comparison of the unadjusted Blue Lake varve thickness measurements with the Devon and Agassiz Ice Cap $\delta^{18}O$ record.

Measured $\delta^{18}O$ values from the Greenland Ice Sheet Project 2 (GISP2), drilled at Summit, Greenland, provided continuous, high-resolution, isotopic information to mean annual temperature change and recorded the Medieval Warm Period and the LIA from 818 AD to 1985 AD (Figure 5.6). $\delta^{18}O$ values for summer and winter showed a reduction of 1.0 and 0.8 ‰ between the years 975 AD and 1720 AD. Decreasing $\delta^{18}O$ values indicate a cooling climate while increasing values indicate a warming climate. This reduction appears to represent the shift from the MWP to the LIA. Indicated by the GISP2 $\delta^{18}O$ measurements, the MWP occurred from 900 AD to 1350 AD and the LIA interval occurred between the years 1350 AD to 1800 AD (Stuiver et al., 1995).

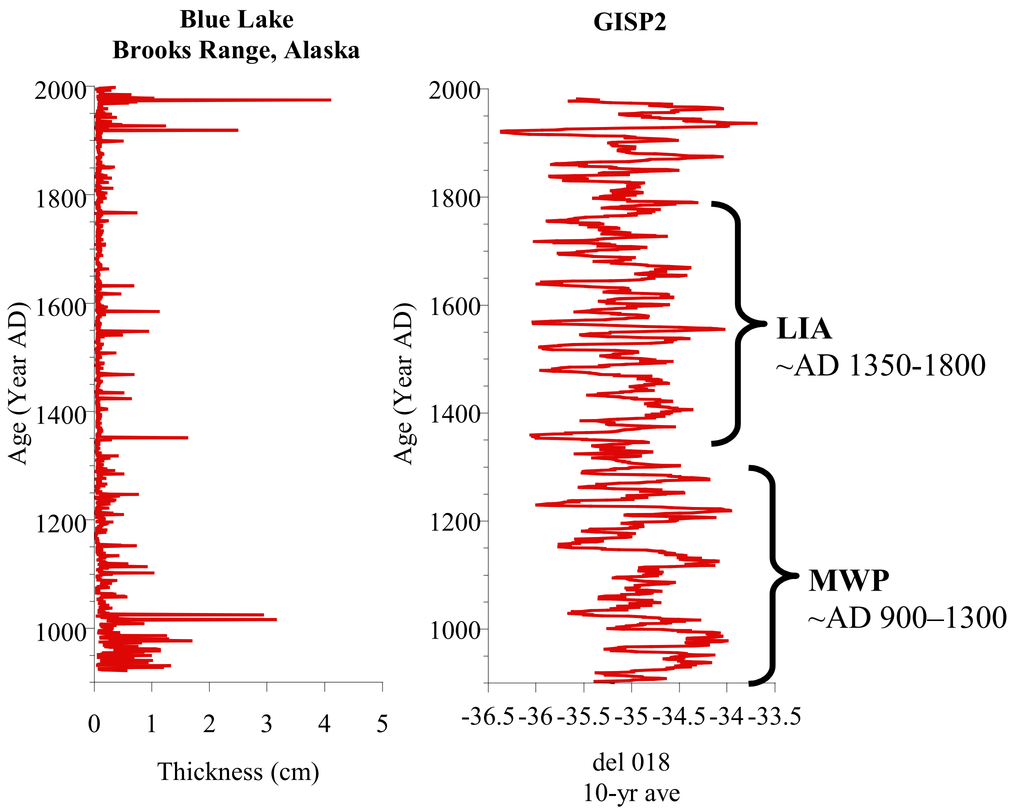

Figure 5.6: The GISP $\delta^{18}O$ record in comparison to the Blue Lake record.

5.4.2 Arctic Lakes

The varve thickness record from Blue Lake corresponds to cooling and warming trends suggested by Arctic lake records (Lamoureux and Bradley, 1996; Hughen et al., 2000; Moore et al., 2001; Lamoureux et al., 2004; Smith et al., 2004). For instance, during the MWP, the varve thickness record from Donard Lake suggests warm decades from ~ 1000 AD to 1100 AD (Figure 5.7). Donard Lake, situated in the Cape Dryer region of Baffin Island, experiences strong seasonal fluctuations in runoff and sediment flux as a result of summer melting of the Caribou Glacier. Two colder periods were recorded from 1000 AD to 1050 AD and from 1150 AD to

1200 AD. The record shows summer temperatures rising from the early 1200's until the middle 1300's (Moore et al., 2001). This warming, suggested by both Blue Lake and Donard Lake varve thicknesses, corresponds to the period when the Thule Inuit moved into the Canadian Arctic from Alaska using open boats and hunting whale (Sutherland, 1992). Radiocarbon dated charcoal from a Thule camp (Hattersley-Smith, 1973) and driftwood samples (Stewart and England, 1983), suggest a period of open water conditions and therefore warmer temperatures during that time.

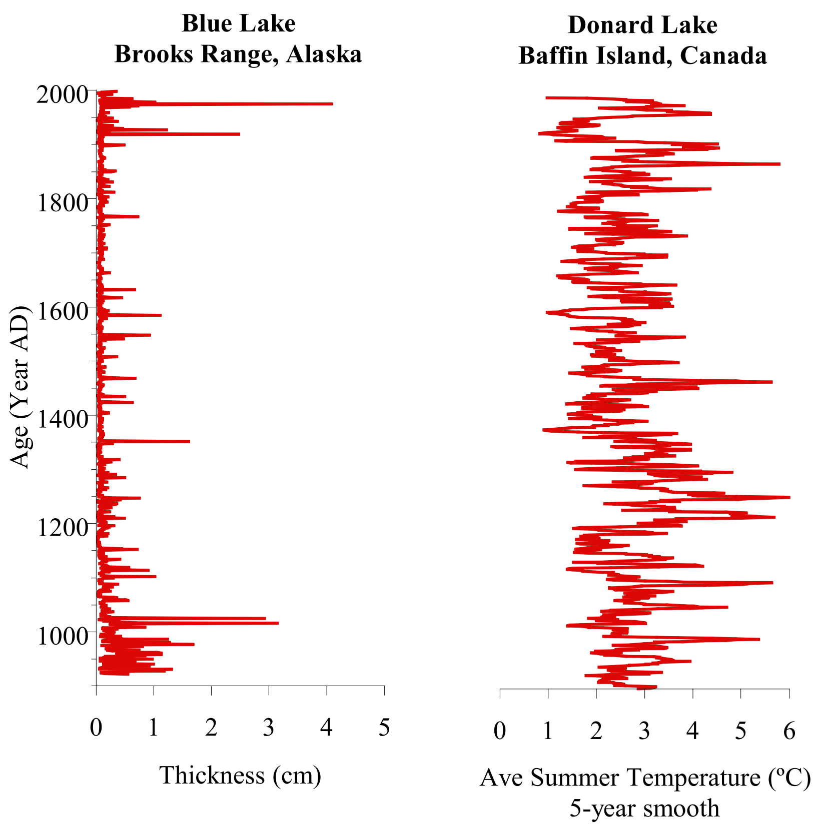

Figure 5.7: Comparison of the Blue Lake varve thickness record with the Donard Lake average summer temperature record.

Most Arctic lake records also suggest several cold centuries prior to the 1900's, during the period corresponding to the LIA (Figure 5.8). The warm period at Donard Lake abruptly ended after 1375 AD, shifting into one of the coldest decades in the record, representing the onset of a 400 year cold phase corresponding to the LIA (Moore et al., 2001). Lake C2, located on the north coast of Ellesmere Island adjacent to the Arctic Ocean, experienced the coldest conditions during the last 1000 years during the 17th and 19th centuries with warmer conditions occurring between ~1400 AD and 1550 AD, 1750 AD to 1800 AD (Lamoureux and Bradley, 1996). Upper Soper Lake, located within the tidal limit on southern Baffin Island on the northern shore of Hudson strait, experienced the coldest conditions from 1700 AD to 1920 AD. Anderson et al. (2001) combined the records from Meli and Tangled Up lakes, located on opposite sides of the Brooks Range, to identify frequent cold conditions between ~1600 AD and 1880 AD.

The varved record at Lake Tuborg (Smith et al., 2004) and Lake C2 (Lamoureux and Bradley, 1996) suggest a significant warming following the middle 19th and early 20th century. The Donard Lake record exhibits an abrupt cooling beginning around 1900 AD, followed by ~50 years of cold temperatures analogous to the LIA. This cold period was followed by dramatic, rapid warming in the 1950's leading to a peak around 1960 AD followed by cooler conditions toward present. Instrumental records of average summer temperature from western Greenland demonstrate similar trends including a gradual warming from 1866 AD to 1900 AD followed by cooling. Particularly high temperatures were observed around 1960 AD followed by an abrupt drop and cooler temperatures in the 1970's and 1980's (Moore et al., 2001). Paleotemperature records from around the circum-Arctic and Northern Hemisphere indicate a warming trend beginning in the 1920s (Overpeck et al., 1997; Mann et al., 1998). There is, however, some divergence between many of the records, particularly in the last 20 to 30 years (Lamoureux et al., 2004). For example, Upper Soper Lake's coldest period abruptly ended with dramatic warming ~1920 AD (Hughen et al., 2000) while Moore et al (2001) shows a more complex pattern (Lamoureux et al., 2004). Blue Lake and Donard Lake exhibit a cooler period during Upper Soper Lake's warming. Blue Lake and Donard Lake suggest warmer periods prior to the 1920's and following the 1950's.

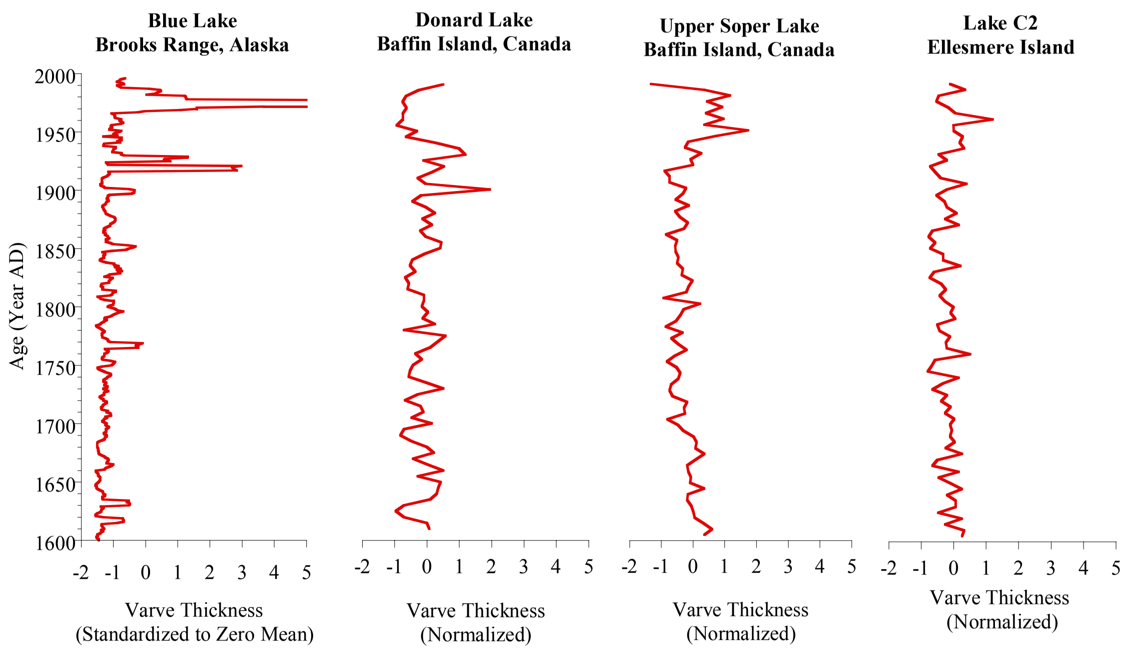

Figure 5.8: Comparison of Blue Lake record with Arctic-wide lake records showing the timing of several cold centuries prior to the 1900's followed by a warming trend.

5.4.3 Northern Alaskan Tree-Ring Temperature Reconstructions

Tree-ring width values and maximum-latewood density values from four sampling sites in northern Alaska were used to reconstruct summer mean temperatures (May to August) (Figure 5.9) (Jacoby et al., 1999; D'Arrigo et al, 2004). The tree-ring sampling sites include 412 (FTR), Arrigetch (ARR), Savage River (SRV) and Twelve Mile Summit (TMS) (Jacoby et al., 1999). Tree-ring reconstructions (Figure 5.10) demonstrate increasingly warmer summers over the last ~100 years (Jacoby and D'Arrigo, 1989; D'Arrigo and Jacoby, 1992, 1993, 1999; Jacoby et al., 1999; Barber et al., 2003). May-August temperature reconstructions based on maximum latewood density data show warm conditions in the late 1600's, near-average conditions in the 1700's and cooler conditions in the 1800's. The mid-20th century (1949 to 1968 AD) appears to be the warmest interval in the reconstruction since 1670 AD (D'Arrigo et al., 2004). Published reconstructions indicate that warming in the mid-19th century gradually continued until the 1920's when warming became more pronounced (Jacoby and D'Arrigo, 1989; Overpeck et al., 1997). The tree-ring studies suggest that cooling trends in Alaska were spatially variable with more severe effects appearing in the interior and northern regions of Alaska (Jacoby et al., 1999). The Blue Lake record suggests a warming beginning in the mid-1850's corresponding to the published reconstructions (Jacoby and D'Arrigo, 1989; Overpeck et al., 1997).

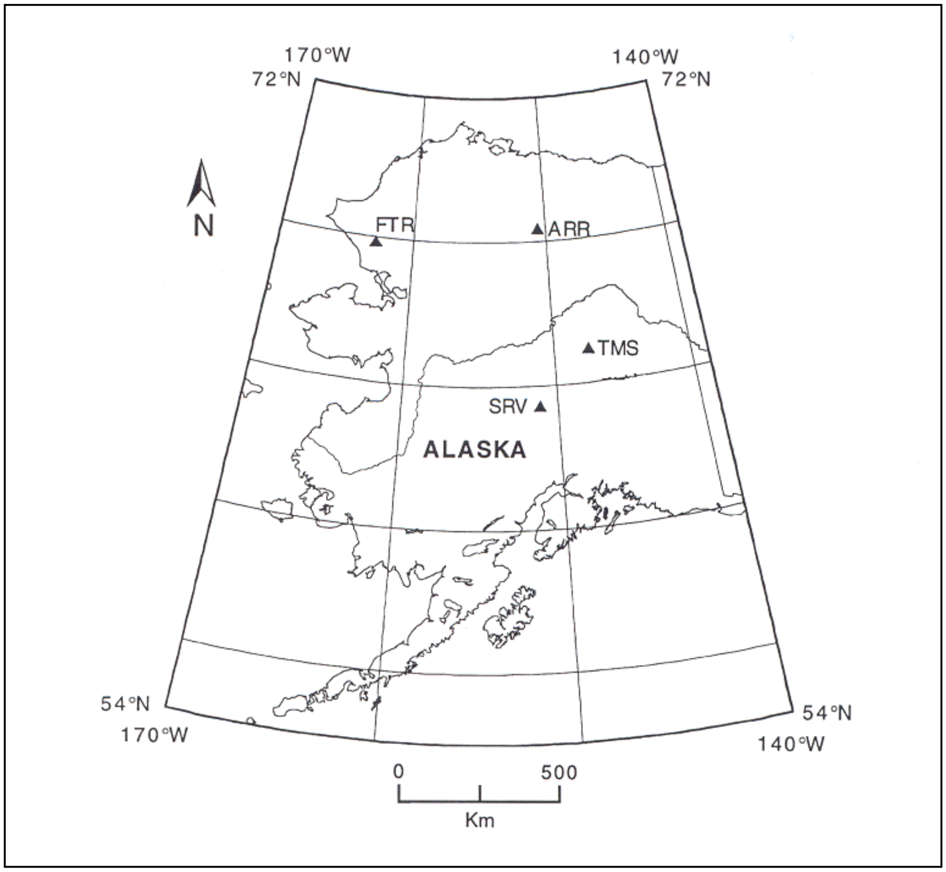

Figure 5.9: Location figure for tree-ring sampling sites in northern Alaska used to reconstruct summer mean temperatures (modified from Jacoby et al., 1999).

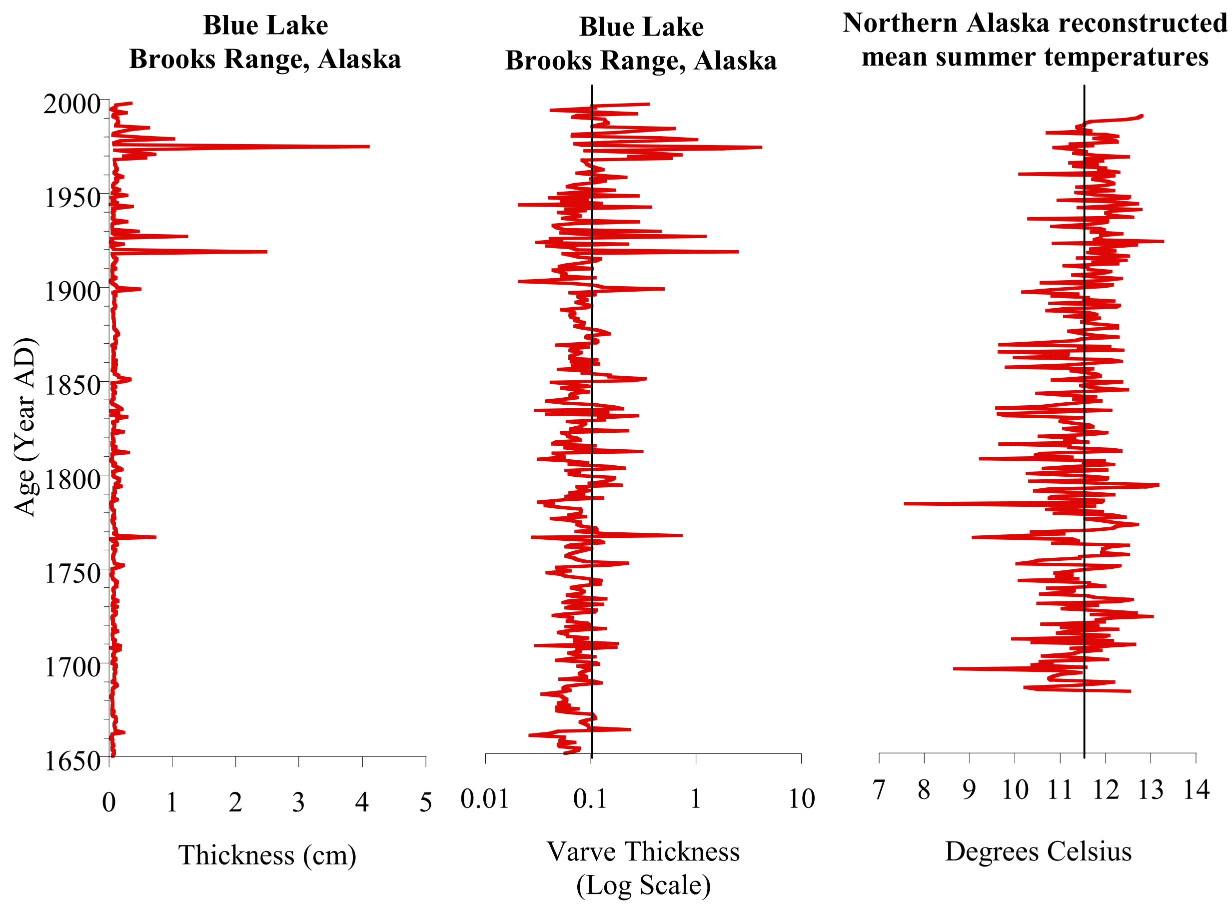

Figure 5.10: Reconstructed temperatures from Northern Alaska compared to the Blue Lake record.

Summer (May to August) temperature reconstruction from Barber et al. (2003) at Fairbanks, Alaska differs from other records of northern hemisphere temperatures yet shows agreement with the Fairbanks instrumental record. Barber et al. (2003) used maximum latewood density and $\delta^{13}C$ discrimination of Interior Alaska white spruce at Fairbanks for the period from 1800 to 1996 AD. Barber et al. (2003) stated that current literature is dominated by tree-ring studies that display a positive-ring-width response to summer temperature (Jacoby and D'Arrigo, 1989) yet trees across the high northern latitudes have become less sensitive to temperatures and suggested that moisture may be the factor controlling tree-ring growth. In contrast, most Northern Hemisphere temperature reconstructions which show low temperatures in the earlier part of the 19th century and a warming in the mid-19th century (Jacoby and D'Arrigo, 1989; Mann et al., 1998; Overpeck et al., 1997), Barber et al. (2003) noted that the early part of the 20th century, from 1916 to 1937 AD, is the coolest period of the 200-year summer temperature reconstruction, suggesting that the interior of Alaska may have experienced temperature trends different from overall temperature trends. Northern Hemisphere mean temperatures show a gradual increase in warm season temperatures from the earliest 20th century until the mid-1950s.

5.5 CLIMATE FORCING

There has been considerable discussion about the role of volcanism, solar variability, and atmospheric forcing of CO_2 on decadal to centennial-scale climate variability. Estimates of past climate forcing are used to drive climate model integrations (Mann et al., 2001). Three primary external forcings and their relationship to global climate change are examined. These are 1) the greenhouse gas CO_2, 2) solar irradiance variations and 3) volcanism (Mann et al., 1998).

Examining the relationship between global temperature changes with variations in volcanic aerosols, solar irradiance and greenhouse-gas concentrations over the same period of time suggest that they all have played a role in climate change over the past several centuries, with greenhouse gases appearing to emerge as the dominant forcing during the 20th century" (Mann et al., 1999).

5.5.1 Volcanic Forcing

Volcanic eruptions eject particulates, gases and vapors into the atmosphere that partially intercept the sun's radiation. This "dust veil" of particulates and aerosols can spread and cover the hemisphere in which they erupted as quickly as six months and can hover above the Earth for a decade or more. The Dust Veil Index (DVI) is a scale that ranks volcanic dust veils by the amount of material ejected, the length of stay in the stratosphere, and the extent of the spread of the veil (Lamb, 1995). The volcanic explosivity index (VEI) is a measure of the magnitude of an eruption without taking into consideration of atmospheric aerosol production (Newhall et al., 1982; Briffa et al., 1998).

The most significant impact from volcanic eruptions on climate is the sulfur-rich gases emitted during the eruption. These gases hydrate into acid crystals and in turn reflect the sun's radiation from the troposphere (Minnis et al., 1993; Jacoby et al., 1999). Sulfate measurements from a number of high latitude ice cores indicate good agreement with estimates of volcanic forcing over the last 600 years (Crowley et al., 1999). Cooling from volcanism is significant in the early 19th century and may have contributed to cooling events in the middle 15th and early 17th centuries as well (Crowley et al., 1999). The GISP2 (Greenland Ice Sheet Project Two) ice core, extracted from Summit, Greenland (72.6ºN, 38.5°W) provided a continuous record of past volcanism. Records of past volcanism, specifically SO_4^{2-} concentrations, from the GISP 2 ice core have been used to study the effects (both magnitude and duration) of volcanic forcing on climate (Zielinski et al., 1994). Concentrations of SO_4^{2-} are a direct measure of the deposition of volcanically produced H_2SO_4, (considered the most important volcanic aerosol climatically).

The distribution of aerosols from large volcanic eruptions is global and is recorded in the continuous Greenland ice core. A time lag of at least 2 years can exist between an eruption and the deposition of aerosols in Greenland. The actual length of the time lag depends on the latitude of the erupting volcano and the season in which the eruption occurred. For example, longer time lags are expected for equatorial eruptions (which are farther from Greenland) and for eruptions occurring in the summer months when there is less mixing between tropical and polar air masses (Zielinski et al., 1994). The GSIP2 volcanic sulfate record (Figure 5.11) shows that volcanic activity has a significant impact on temperature at high latitudes. The reconstructed atmospheric volcanic sulfate loading from GISP 2 corresponds to a cooling of the circum-Arctic (Overpeck et al., 1997). It is important to note that during the timing of the LIA, there was a significant increase in volcanism that may have attributed to the cooling trend. For example in 1783 AD there were two large explosive eruptions, one in Ireland and the other in Japan. The effects of the two eruptions corresponded with a cooling of 1 to 2°C during that time period (Jacoby et al., 1999).

Tree-ring records from the northern hemisphere agree, indicating that volcanic eruptions are a significant factor in temperature variations in the northern hemisphere (Nesje and Dahl, 2000). Important to the Blue Lake record has been the northern Alaskan tree-ring reconstruction, which has proved to be valuable in studying the effect volcanism has on climate change. Sulfur-producing volcanic eruptions can have a significant cooling effect on a time scale of a few years by reflecting solar radiation. However, direct sulfate measurements provided from ice cores are not always dated precisely (D'Arrigo et al., 1999). The measurements of sulfate in ice cores can also be affected by the latitude and season on eruption (Zielinski et al., 1994). Annually dated tree-ring records have provided a beneficial means to evaluate climate change as a result of volcanic eruptions (D'Arrigo et al., 1999). Density, rather than ring widths, provides a better temperature signal at northern sites because ring widths typically have a weaker summer climate response than density. Higher density values correspond to warmer temperatures during the growth season, lower density values correspond to cooler temperatures (D'Arrigo et al., 1999). Temperature-sensitive tree-ring density measurements are provided by the measurement of the density of the wood cells in annual tree-rings (Jacoby et al., 1999). Results of density data from trees demonstrate that several major volcanic events of recent centuries have been significant climatically and are reflected in extremely low-density tree-ring years. There are on record a few extremes with no known events as well as known events that are not represented by low-density values. Again, this may be due to the differences in the impacts of individual eruptions which vary considerably due to location, timing and type of eruption, and prevailing circulation (D'Arrigo et al., 1999). Northern Alaska tree-ring sampling sites such as Four-Twelve, Arrigetch (67°27' N, 154°03' W), and Twelve-Mile (64°24' N, 145°1857' W), are within the vicinity of Blue Lake and provide a beneficial record for comparison.

5.5.2 Solar Variability

Models estimate that as much as 18-34% of low frequency temperature change could have been forced by volcanism and solar variability for the pre-anthropogenic time period. Anthropogenic forcing (CO_2 and other trace gases) are considered primarily after 1800 AD (Crowley and Kim, 1999). Attempts to reconstruct solar irradiance variations are based on the variance of sunspots, which may be directly observed or inferred from variations in ^{14}C and ^{10}Be in paleoclimate proxies, such as ice cores. The earth's magnetic field is less disturbed during periods of reduced sunspot activity and is therefore better able to protect the atmosphere from the high-energy particles that produce these cosmogenic isotopes (Rind, 2002).

The LIA correlated with a period of time from the mid-1600's to the early 1700's during which there was little or no sunspot activity (solar irradiance) known as the Maunder Minimum (see Figure 5.11) (Shindell et al., 2001). During the Maunder Minimum, solar output was thought to have decreased by approximately 0.25%. This is equivalent a global temperature reduction of about ½ °C" (Nesje and Dahl, 2000). A warming trend then followed as the solar irradiance (sunspot activity) increased from the early 19th century through to the mid 20th century (Mann et al., 1998).

There is some debate of how much climate is influenced by solar variability (Rind, 2002). Overpeck (1997) writes that although the coincidence of high solar irradiance and warm Arctic temperatures in the 18th and 19th centuries suggests solar forcing, he believes that the Maunder Minimum period argues "against a dominant role for solar forcing over the past 400 years". Although average global temperature changes are predicted to be small in climate model and empirical reconstructions, regional temperature changes can be significantly large. GCM and paleoclimate reconstructions indicate that solar forcing affects regional scales more strongly than global or hemispheric scales through forcing of the Arctic Oscillation (AO) and North Atlantic Oscillation (NA). Paleoclimate evidence suggests a shift toward a low-index state during intervals of reduced solar forcing which leads to overall cooler temperatures in the northern Hemisphere. (Shindell et al., 2001).

When the forcing mechanisms of volcanic dust and solar irradiance are combined, they correlate well with the past temperature variations up until approximately 1940 when increased concentrations of trace gases take effect (Overpeck et al., 1997).

5.5.3 Atmospheric CO_2 Concentrations

Increases in atmospheric CO_2 and other greenhouse gas concentrations during the 20th century are an important forcing mechanism resulting in warmer conditions across the northern hemisphere during the last several decades (Mann et al., 1998). Although CO_2 is a trace-gas, its significance is due to the effect it has on solar radiation passing through the atmosphere. Solar radiation, mostly in the form of outgoing long-wave radiation, is absorbed by CO_2 in the atmosphere and re-radiated back to the Earth. As a result, the Earth's surface may become increasingly warm (Lamb, 1995). This forcing, referred to as greenhouse-gas forcing, did not show signs of playing a role in climate forcing of the last millennium until the 20th century when a large positive correlation with temperature dramatically occurred (Figure 5.11) (Mann et al., 1998). Measurements of atmospheric CO_2 did not start until 1958 AD. Prior to 1958 AD air bubbles enclosed within polar ice cores were measured to obtain atmospheric trace gas concentrations (Indermule et al., 1999). Such studies showed atmospheric levels of CO_2 at approximately 290 ppm in 1880 AD (Lamb, 1995). From 1958 AD to 1997 AD there was a clear increase from 315 ppm to 364 ppm. From 1840 AD to 1920 AD, however, concentrations of atmospheric CO_2 increased by only about 20 ppm. This leaves many to believe that greenhouse forcing alone is not enough to explain the pre-1920 warming (Overpeck et al., 1997) but that it has become the dominant force in the 20th century.

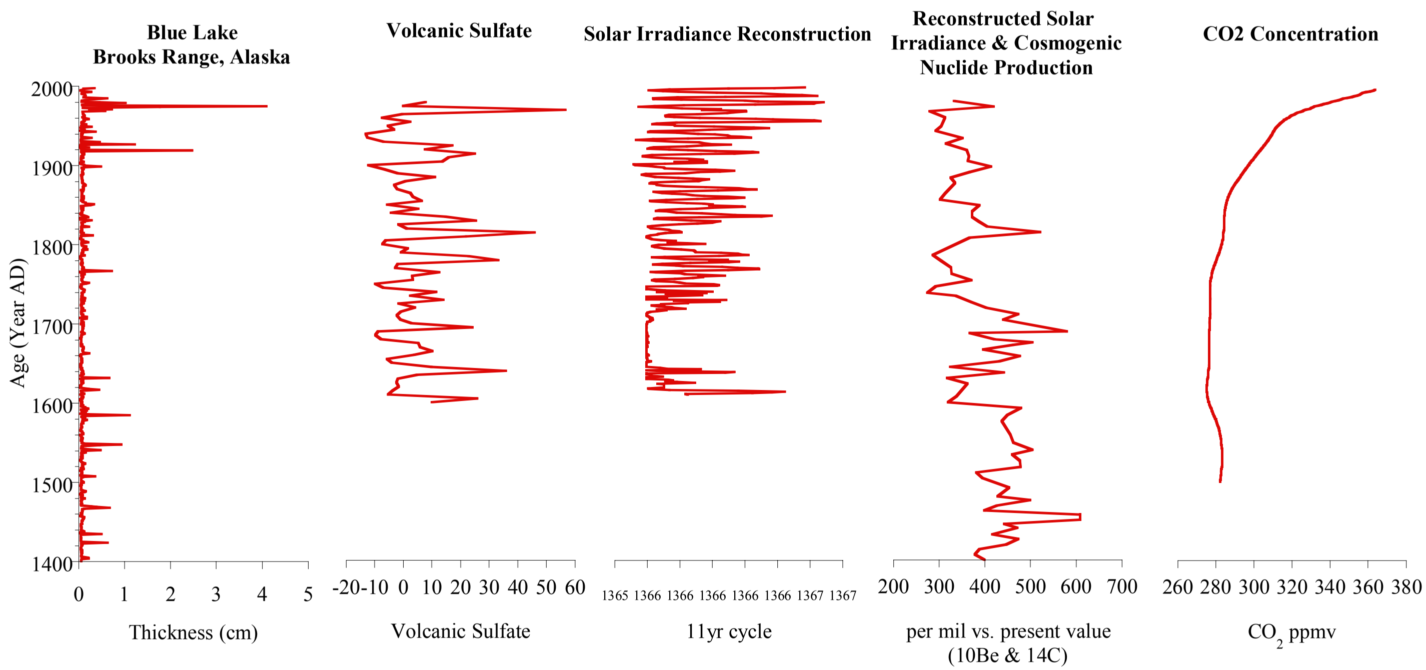

Figure 5.11: External forcings (volcanic aerosols, solar irradiance and greenhouse-gas concentrations) and their relationship to climate change plotted over the same period of time suggesting that they played a role in climate change over the past several centuries.

6.0 CONCLUSIONS AND RECOMMENDATIONS

The Arctic is one of the most susceptible places to both natural and human-induced climate change (Overpeck et al., 1997). Evidence for the LIA can be seen in Greenland, Iceland, Spits Bergen, Scandinavia, Devon Island, and Alaska. The instrumental record during the last 100 years indicates that the Arctic has warmed by as much as 0.6 °C since the beginning of the 20th century. The transition from the cold conditions of the 19th century to the warming trend of the 20th century can be observed in temperature proxy records, including the Blue Lake varve thickness record. The increased Arctic temperatures from approximately 1840 AD to 1920 AD appear to be a "natural readjustment as volcanic forcing weakened and irradiance (and to a lesser extent, greenhouse gases) increased" (Overpeck et al., 1997). After 1920 AD, Arctic climate was increasingly influenced by rising concentrations of atmospheric trace-gases, although high solar irradiance and decreased volcanic dust still played minor roles. Overall, the varve measurements from Blue Lake broadly correlate with regional cooling and warming trends described for the late Holocene. The Blue Lake varve record compares well with middle to high-Arctic climate proxy records. The varved sediments of Blue Lake records the glacial response to late Holocene climate phenomena, such as the LIA (cooling), MWP (warming), and the 20th century warming trend.

The length of the sediment record obtained from Blue Lake was limited by the coring method employed. There is potential to retrieve a much longer sediment core using a different coring system. In light of the potential for producing a longer climate record, the retrieval of additional cores is highly recommended. In addition, hydro-meteorological and sedimentological monitoring for establishing a base for climate-varve interpretations is also important.

APPENDIX

VARVE THICKNESS MEASUREMENTS

Year AD	Thickness (cm)	Year AD	Thickness (cm)
1999	1.2259	1966	0.0918
1998	0.3510	1965	0.1006
1997	0.1023	1964	0.1112
1996	0.1111	1963	0.1306
1995	0.0423	1962	0.1077
1994	0.1023	1961	0.0741
1993	0.2716	1960	0.1218
1992	0.0758	1959	0.2153
1991	0.0670	1958	0.1006
1990	0.1358	1957	0.1377
1989	0.1380	1956	0.1130
1988	0.1469	1955	0.0706
1987	0.1191	1954	0.0600
1986	0.1032	1953	0.0794
1985	0.6226	1952	0.1677
1984	0.3316	1951	0.0794
1983	0.1676	1950	0.0495
1982	0.0680	1949	0.2798
1981	0.0663	1948	0.0406
1980	0.4525	1947	0.0918
1979	1.0132	1946	0.0530
1978	0.1906	1945	0.1253
1977	0.0706	1944	0.0212
1976	0.0847	1943	0.3707
1975	4.0879	1942	0.0582
1974	1.7686	1941	0.0883
1973	0.0883	1940	0.0494
1972	0.3777	1939	0.0715
1971	0.7240	1938	0.0794
1970	0.2259	1937	0.0539
1969	0.5807	1936	0.0768
1968	0.0830	1935	0.2820
1967	0.0900	1934	0.0653

Year AD	Thickness (cm)
1933	0.0441
1932	0.0477
1931	0.0547
1930	0.4581
1929	0.0521
1928	0.1011
1927	1.2175
1926	0.0415
1925	0.0525
1924	0.0309
1923	0.2229
1922	0.0384
1921	0.0640
1920	0.0742
1919	2.4694
1918	0.0547
1917	0.0653
1916	0.0777
1915	0.1236
1914	0.1094
1913	0.0830
1912	0.0600
1911	0.0503
1910	0.1033
1909	0.0441
1908	0.0530
1907	0.0582
1906	0.0530
1905	0.1094
1904	0.0424
1903	0.0212
1902	0.0671
1901	0.1112
1900	0.1306
1899	0.4854
1898	0.1289
1897	0.0635
1896	0.1094
1895	0.0759
1894	0.0830
1893	0.0918
1892	0.0724
1891	0.0847
1890	0.1024
1889	0.0883

Year AD	Thickness (cm)
1888	0.0530
1887	0.0671
1886	0.0706
1885	0.0635
1884	0.0653
1883	0.0759
1882	0.0706
1881	0.0865
1880	0.0847
1879	0.0706
1878	0.0847
1877	0.1147
1876	0.1306
1875	0.1483
1874	0.0935
1873	0.0900
1872	0.1077
1871	0.1165
1870	0.1112
1869	0.0477
1868	0.0953
1867	0.0671
1866	0.0635
1865	0.0812
1864	0.0741
1863	0.0635
1862	0.0635
1861	0.1147
1860	0.0653
1859	0.1183
1858	0.0671
1857	0.0988
1856	0.0494
1855	0.0971
1854	0.0830
1853	0.1536
1852	0.1483
1851	0.3274
1850	0.2506
1849	0.0424
1848	0.0653
1847	0.1006
1846	0.0530
1845	0.0715
1844	0.0953

Year AD	Thickness (cm)
1843	0.0671
1842	0.0635
1841	0.0741
1840	0.0556
1839	0.0379
1838	0.0565
1837	0.1077
1836	0.1624
1835	0.2008
1834	0.0300
1833	0.1456
1832	0.0379
1831	0.2771
1830	0.1200
1829	0.1359
1828	0.0600
1827	0.0900
1826	0.0830
1825	0.0794
1824	0.0644
1823	0.2224
1822	0.0530
1821	0.0618
1820	0.0609
1819	0.0733
1818	0.0794
1817	0.0477
1816	0.0432
1815	0.1094
1814	0.0574
1813	0.0794
1812	0.3054
1811	0.0441
1810	0.0530
1809	0.0556
1808	0.0318
1807	0.0609
1806	0.0936
1805	0.0627
1804	0.1456
1803	0.2083
1802	0.0582
1801	0.0777
1800	0.0627
1799	0.0750

Year AD	Thickness (cm)
1798	0.1686
1797	0.1606
1796	0.1341
1795	0.0971
1794	0.1942
1793	0.0741
1792	0.0794
1791	0.0971
1790	0.0635
1789	0.0847
1788	0.0582
1787	0.1296
1786	0.0547
1785	0.0318
1784	0.0441
1783	0.0371
1782	0.0530
1781	0.0794
1780	0.0812
1779	0.0794
1778	0.0618
1777	0.0900
1776	0.0424
1775	0.0618
1774	0.0794
1773	0.0741
1772	0.0830
1771	0.1094
1770	0.1147
1769	0.0724
1768	0.1289
1767	0.7260
1766	0.0282
1765	0.0565
1764	0.1183
1763	0.1324
1762	0.0653
1761	0.0582
1760	0.1024
1759	0.0865
1758	0.0741
1757	0.0635
1756	0.0583
1755	0.0688
1754	0.0741

Year AD	Thickness (cm)	Year AD	Thickness (cm)
1753	0.0900	1708	0.0300
1752	0.2224	1707	0.1730
1751	0.1518	1706	0.0741
1750	0.0477	1705	0.0794
1749	0.0494	1704	0.0618
1748	0.0635	1703	0.0724
1747	0.0388	1702	0.1094
1746	0.0530	1701	0.0653
1745	0.0582	1700	0.0477
1744	0.0918	1699	0.1094
1743	0.1253	1698	0.1183
1742	0.1006	1697	0.0759
1741	0.1236	1696	0.0953
1740	0.0847	1695	0.1006
1739	0.0653	1694	0.0846
1738	0.0794	1693	0.0777
1737	0.0865	1692	0.0847
1736	0.0812	1691	0.0909
1735	0.0600	1690	0.0512
1734	0.0706	1689	0.1024
1733	0.1394	1688	0.1253
1732	0.0635	1687	0.0759
1731	0.0547	1686	0.0582
1730	0.1298	1685	0.0547
1729	0.0671	1684	0.0635
1728	0.0582	1683	0.0538
1727	0.1130	1682	0.0344
1726	0.1077	1681	0.0530
1725	0.0583	1680	0.0547
1724	0.0441	1679	0.0591
1723	0.0671	1678	0.0582
1722	0.0653	1677	0.0494
1721	0.0600	1676	0.0618
1720	0.0918	1675	0.0477
1719	0.0971	1674	0.0759
1718	0.0582	1673	0.0477
1717	0.1377	1672	0.0635
1716	0.0653	1671	0.1041
1715	0.0494	1670	0.1077
1714	0.0600	1669	0.1112
1713	0.0600	1668	0.0918
1712	0.0936	1667	0.0794
1711	0.0706	1666	0.0900
1710	0.0706	1665	0.0953
1709	0.1783	1664	0.0953

Year AD	Thickness (cm)
1663	0.2330
1662	0.0494
1661	0.0424
1660	0.0265
1659	0.0565
1658	0.0547
1657	0.0512
1656	0.0706
1655	0.0494
1654	0.0512
1653	0.0777
1652	0.0759
1651	0.0653
1650	0.0547
1649	0.0388
1648	0.0547
1647	0.0441
1646	0.0406
1645	0.0441
1644	0.0688
1643	0.0477
1642	0.0724
1641	0.0900
1640	0.0953
1639	0.0759
1638	0.0582
1637	0.1094
1636	0.0865
1635	0.0371
1634	0.0759
1633	0.0741
1632	0.6672
1631	0.0353
1630	0.0953
1629	0.0918
1628	0.0494
1627	0.0653
1626	0.1006
1625	0.0741
1624	0.0600
1623	0.0547
1622	0.0353
1621	0.0388
1620	0.0406
1619	0.0671

Year AD	Thickness (cm)
1618	0.2189
1617	0.4483
1616	0.0441
1615	0.0565
1614	0.0600
1613	0.0812
1612	0.1200
1611	0.0388
1610	0.0777
1609	0.0688
1608	0.1041
1607	0.0582
1606	0.0847
1605	0.0379
1604	0.0415
1603	0.0477
1602	0.0741
1601	0.0459
1600	0.0530
1599	0.0759
1598	0.0512
1597	0.0953
1596	0.0424
1595	0.1403
1594	0.1077
1593	0.2136
1592	0.0441
1591	0.1765
1590	0.0635
1589	0.1006
1588	0.1500
1587	0.0388
1586	0.2118
1585	1.1120
1584	0.0918
1583	0.0618
1582	0.1430
1581	0.1024
1580	0.0830
1579	0.1765
1578	0.0935
1577	0.0741
1576	0.0706
1575	0.1041
1574	0.0671

Year AD	Thickness (cm)
1573	0.0494
1572	0.0530
1571	0.0565
1570	0.0706
1569	0.0565
1568	0.0459
1567	0.0565
1566	0.0406
1565	0.0547
1564	0.0759
1563	0.0741
1562	0.1024
1561	0.0953
1560	0.0353
1559	0.0530
1558	0.0635
1557	0.0494
1556	0.0918
1555	0.0706
1554	0.0530
1553	0.0424
1552	0.0777
1551	0.0759
1550	0.0635
1549	0.1165
1548	0.9285
1547	0.4519
1546	0.0724
1545	0.0600
1544	0.0900
1543	0.0547
1542	0.1553
1541	0.4748
1540	0.0653
1539	0.0812
1538	0.1553
1537	0.0494
1536	0.0706
1535	0.0618
1534	0.0830
1533	0.0494
1532	0.0459
1531	0.0847
1530	0.0583
1529	0.0512

Year AD	Thickness (cm)
1528	0.0300
1527	0.0565
1526	0.0600
1525	0.0812
1524	0.1403
1523	0.1103
1522	0.0688
1521	0.0741
1520	0.0803
1519	0.0980
1518	0.0477
1517	0.1112
1516	0.0494
1515	0.0344
1514	0.0733
1513	0.0635
1512	0.0741
1511	0.0600
1510	0.0582
1509	0.0406
1508	0.3557
1507	0.1041
1506	0.0485
1505	0.0530
1504	0.0547
1503	0.0530
1502	0.0582
1501	0.0812
1500	0.1112
1499	0.0459
1498	0.0653
1497	0.0671
1496	0.0388
1495	0.0600
1494	0.0512
1493	0.0618
1492	0.0618
1491	0.0477
1490	0.0900
1489	0.1500
1488	0.1306
1487	0.0477
1486	0.0724
1485	0.0282
1484	0.0900

Year AD	Thickness (cm)
1483	0.0741
1482	0.0547
1481	0.0477
1480	0.1359
1479	0.0600
1478	0.0688
1477	0.0424
1476	0.0671
1475	0.0538
1474	0.0521
1473	0.0688
1472	0.0424
1471	0.0565
1470	0.2754
1469	0.3795
1468	0.6725
1467	0.1324
1466	0.0724
1465	0.0688
1464	0.0865
1463	0.0724
1462	0.0759
1461	0.0477
1460	0.0582
1459	0.0688
1458	0.0353
1457	0.0565
1456	0.1236
1455	0.1006
1454	0.1077
1453	0.0830
1452	0.0918
1451	0.0671
1450	0.0653
1449	0.0653
1448	0.0777
1447	0.0459
1446	0.0530
1445	0.0441
1444	0.0547
1443	0.0635
1442	0.0583
1441	0.0565
1440	0.0459
1439	0.0741

Year AD	Thickness (cm)
1438	0.1236
1437	0.0371
1436	0.0265
1435	0.4942
1434	0.0441
1433	0.0468
1432	0.0424
1431	0.0432
1430	0.0583
1429	0.0459
1428	0.0441
1427	0.0468
1426	0.0530
1425	0.0600
1424	0.6308
1423	0.0505
1422	0.0847
1421	0.0783
1420	0.0642
1419	0.0512
1418	0.0512
1417	0.0459
1416	0.0477
1415	0.0635
1414	0.0738
1413	0.0494
1412	0.0494
1411	0.0741
1410	0.0618
1409	0.0635
1408	0.0635
1407	0.0547
1406	0.0706
1405	0.2065
1404	0.2153
1403	0.0635
1402	0.0582
1401	0.0547
1400	0.0635
1399	0.0477
1398	0.0759
1397	0.0671
1396	0.0582
1395	0.0794
1394	0.1112

Year AD	Thickness (cm)
1393	0.1006
1392	0.1077
1391	0.0600
1390	0.1041
1389	0.0830
1388	0.0706
1387	0.0971
1386	0.0582
1385	0.0583
1384	0.0600
1383	0.0530
1382	0.0706
1381	0.0477
1380	0.0494
1379	0.1059
1378	0.0512
1377	0.0512
1376	0.0618
1375	0.0706
1374	0.0424
1373	0.0759
1372	0.0459
1371	0.0583
1370	0.0865
1369	0.1130
1368	0.0794
1367	0.0971
1366	0.1236
1365	0.0741
1364	0.1289
1363	0.0988
1362	0.1024
1361	0.0741
1360	0.0741
1359	0.0671
1358	0.0918
1357	0.0424
1356	0.0671
1355	0.0935
1354	0.0565
1353	0.0512
1352	1.6010
1351	0.1906
1350	0.2012
1349	0.2259

Year AD	Thickness (cm)
1348	0.2807
1347	0.0424
1346	0.0424
1345	0.0847
1344	0.0388
1343	0.0177
1342	0.0371
1341	0.0388
1340	0.0812
1339	0.0424
1338	0.0600
1337	0.0406
1336	0.0441
1335	0.0565
1334	0.0424
1333	0.0600
1332	0.0759
1331	0.0406
1330	0.0424
1329	0.0441
1328	0.0547
1327	0.0459
1326	0.0353
1325	0.0441
1324	0.0477
1323	0.1059
1322	0.0635
1321	0.0512
1320	0.0494
1319	0.0900
1318	0.3988
1317	0.0962
1316	0.0626
1315	0.0750
1314	0.2547
1313	0.1244
1312	0.1323
1311	0.0529
1310	0.0388
1309	0.1491
1308	0.0864
1307	0.0670
1306	0.0776
1305	0.0811
1304	0.0600

Year AD	Thickness (cm)
1303	0.0847
1302	0.1429
1301	0.0917
1300	0.0723
1299	0.0952
1298	0.0494
1297	0.0864
1296	0.1323
1295	0.1270
1294	0.2011
1293	0.0600
1292	0.0494
1291	0.3360
1290	0.0370
1289	0.0353
1288	0.0582
1287	0.1094
1286	0.0944
1285	0.4940
1284	0.0688
1283	0.0714
1282	0.0882
1281	0.0811
1280	0.1191
1279	0.1094
1278	0.0926
1277	0.1887
1276	0.0617
1275	0.0353
1274	0.1005
1273	0.0688
1272	0.0582
1271	0.0582
1270	0.1094
1269	0.0724
1268	0.0618
1267	0.0653
1266	0.1959
1265	0.0794
1264	0.0812
1263	0.1659
1262	0.0388
1261	0.0327
1260	0.0830
1259	0.0432

Year AD	Thickness (cm)
1258	0.0653
1257	0.0441
1256	0.0459
1255	0.0618
1254	0.0335
1253	0.0459
1252	0.1165
1251	0.0512
1250	0.0459
1249	0.0618
1248	0.2365
1247	0.7502
1246	0.1659
1245	0.1112
1244	0.4210
1243	0.2383
1242	0.0291
1241	0.0265
1240	0.0406
1239	0.0653
1238	0.1995
1237	0.3548
1236	0.2248
1235	0.3283
1234	0.1006
1233	0.0830
1232	0.0547
1231	0.2559
1230	0.2542
1229	0.2171
1228	0.0741
1227	0.0900
1226	0.0688
1225	0.0688
1224	0.0812
1223	0.0530
1222	0.2365
1221	0.0406
1220	0.0371
1219	0.0441
1218	0.1041
1217	0.0918
1216	0.0318
1215	0.0618
1214	0.0388

Year AD	Thickness (cm)
1213	0.3018
1212	0.0229
1211	0.0847
1210	0.4925
1209	0.0424
1208	0.1094
1207	0.0759
1206	0.0459
1205	0.0477
1204	0.1289
1203	0.1589
1202	0.1730
1201	0.1165
1200	0.1041
1199	0.0988
1198	0.0847
1197	0.0459
1196	0.3071
1195	0.1271
1194	0.2224
1193	0.1112
1192	0.1995
1191	0.1341
1190	0.1359
1189	0.0918
1188	0.0988
1187	0.0688
1186	0.1147
1185	0.0600
1184	0.0371
1183	0.0477
1182	0.0582
1181	0.2030
1180	0.0459
1179	0.0388
1178	0.1553
1177	0.1889
1176	0.0459
1175	0.0300
1174	0.0371
1173	0.0247
1172	0.0282
1171	0.0353
1170	0.0318
1169	0.0300

Year AD	Thickness (cm)
1168	0.0300
1167	0.0353
1166	0.0353
1165	0.0565
1164	0.0415
1163	0.0415
1162	0.0547
1161	0.0635
1160	0.0494
1159	0.0370
1158	0.0441
1157	0.0600
1156	0.0688
1155	0.0706
1154	0.4445
1153	0.3828
1152	0.7161
1151	0.1305
1150	0.0494
1149	0.1023
1148	0.0441
1147	0.0777
1146	0.0803
1145	0.1262
1144	0.0583
1143	0.0900
1142	0.0441
1141	0.0953
1140	0.0512
1139	0.1712
1138	0.1024
1137	0.0671
1136	0.0706
1135	0.1183
1134	0.4113
1133	0.1536
1132	0.1836
1131	0.1871
1130	0.1677
1129	0.1059
1128	0.1006
1127	0.0900
1126	0.0644
1125	0.1103
1124	0.1103

Year AD	Thickness (cm)
1123	0.1712
1122	0.1597
1121	0.1950
1120	0.2030
1119	0.5666
1118	0.0847
1117	0.2321
1116	0.1112
1115	0.3292
1114	0.9037
1113	0.2912
1112	0.1289
1111	0.2215
1110	0.0944
1109	0.1059
1108	0.0583
1107	0.0918
1106	0.1059
1105	0.1289
1104	0.0900
1103	0.3107
1102	1.0149
1101	0.1359
1100	0.3001
1099	0.1147
1098	0.1130
1097	0.0794
1096	0.0521
1095	0.0468
1094	0.0759
1093	0.0680
1092	0.0627
1091	0.0997
1090	0.0847
1089	0.0635
1088	0.3769
1087	0.2012
1086	0.1289
1085	0.2736
1084	0.1412
1083	0.2807
1082	0.1518
1081	0.1218
1080	0.1465
1079	0.2171

Year AD	Thickness (cm)
1078	0.1341
1077	0.0812
1076	0.0635
1075	0.2471
1074	0.0477
1073	0.0441
1072	0.0371
1071	0.0371
1070	0.0768
1069	0.0715
1068	0.0388
1067	0.0477
1066	0.0424
1065	0.0724
1064	0.2948
1063	0.3530
1062	0.1341
1061	0.3301
1060	0.3212
1059	0.5013
1058	0.5542
1057	0.1394
1056	0.1130
1055	0.1341
1054	0.0724
1053	0.0724
1052	0.1059
1051	0.1006
1050	0.1147
1049	0.1712
1048	0.0988
1047	0.1165
1046	0.0883
1045	0.1694
1044	0.1606
1043	0.1305
1042	0.2381
1041	0.1305
1040	0.1252
1039	0.1041
1038	0.1834
1037	0.2946
1036	0.1252
1035	0.1393
1034	0.1270

Year AD	Thickness (cm)	Year AD	Thickness (cm)
1033	0.0864	988	0.4304
1032	0.1341	987	0.3228
1031	0.1411	986	1.2400
1030	0.1711	985	0.2619
1029	0.0864	984	0.1332
1028	0.2381	983	0.1146
1027	0.1376	982	0.1217
1026	0.5080	981	0.3457
1025	2.9175	980	1.2682
1024	0.4163	979	0.2752
1023	0.0547	978	0.8855
1022	0.1094	977	1.6792
1021	0.2769	976	0.4516
1020	0.1358	975	0.0952
1019	0.4004	974	0.3687
1018	0.3545	973	0.8070
1017	0.6897	972	0.2320
1016	3.1415	971	0.4507
1015	0.2575	970	0.1834
1014	0.2399	969	0.1694
1013	0.3175	968	0.3265
1012	0.6050	967	0.7466
1011	0.3387	966	0.1977
1010	0.4321	965	0.2930
1009	0.8467	964	0.6619
1008	0.5115	963	0.3583
1007	0.1199	962	1.0414
1006	0.1129	961	1.1332
1005	0.3651	960	1.0102
1004	0.2381	959	0.3565
1003	0.1376	958	1.1297
1002	0.1746	957	0.4077
1001	0.1852	956	0.8472
1000	0.3157	955	0.1589
999	0.2540	954	0.6443
998	0.2028	953	0.1359
997	0.2999	952	0.3742
996	0.0917	951	0.0688
995	0.2910	950	0.9708
994	0.0900	949	0.4519
993	0.0829	948	0.4039
992	0.4233	947	0.0776
991	0.0776	946	0.0688
990	0.2028	945	0.6738
989	0.2910	944	0.2258

Year AD	Thickness (cm)	Year AD	Thickness (cm)
943	0.3457	932	0.0618
942	0.1270	931	1.3106
941	0.9948	930	1.0936
940	0.1305	929	0.7479
939	0.4551	928	1.1836
938	0.3351	927	0.6562
937	0.9137	926	0.0900
936	0.2012	925	0.1746
935	0.1536	924	0.0917
934	0.1024	923	0.1676
933	0.0724	922	0.5503

BIBLIOGRAPHY

Anderson, L., Abbott, M., and Finney, B., 2001. Holocene climate inferred from oxygen isotope ratios in lake sediments, central Brooks Range, Alaska. *Quaternary Research* 55: 313-321.

Anderson, P.M. and Brubaker, L.B., 1993. Holocene vegetation and climate histories of Alaska, *in* Global Climates since the last glacial maximum (H.E. Wright, Jr., et al., Eds.) University of Minnesota Press, 386-400.

Appleby, P.B., Flower, R.J., Mackay, A.W., and Rose, N.L., 1998. Paleolimnological assessment of recent environmental change in Lake Baikal: sediment chronology. *Journal of Paleolimnology* 20: 119-133.

Barber V.A., Juday, G.P., Finney, B.P., and Wilmking, M. 2003. Reconstruction of summer temperatures in interior Alaska from tree-ring proxies: evidence for changing synoptic climate regimes. Climatic Change 00: 1-30.

Barlow, L.K., Sadler, J.P., Ogilivie, A.E.J., Buckland, P.C. Amorosi, T., Ingimundarson, J.H., Skidmore, P., Dugmore, A.J., and McGovern, T.H. 1997. Interdisciplinary investigations of the end of the Norse western settlement in Greenland. *The Holocene* 7: 489-499.

Bartlein P.J., Anderson, P.M., Edwards, M.E., MacDowell, P.F., 1992. A framework for interpreting paleoclimatic variations in eastern Beringia. *Quaternary International* 1012: 73-83.

Binford M.W., Kahl., J.S., and Norton, S.A., 1993. Interpretation of ^{210}Pb profiles and verification of the CRS dating model in PIRLA project lake sediment cores. *Journal of Paleolimnology* 9: 275-296.

Bourgeois, J.C., Koerner, R.J., Gajewski, K., and Fisher, D.A. 2000. A Holocene ice-core pollen record from Ellesmere Island, Nunavut, Canada. *Quaternary Research* 54: 275-283.

Bradley, R.S. 2000. Past global changes and their significance for the future. *Quaternary Science Reviews* 19: 391-402.

Bradley, R.S., 1990. Holocene paleoclimatology of the Queen Elizabeth Islands, Canadian High Arctic. *Quaternary Science Reviews* 9: 365-384.

Bradley, R.S., and Jones, P.D., 1992. Climate since AD 1500: Introduction, *In* "Climate since AD 1500" (Bradley, R.S. and Jones, P.D., *Eds.), Routledge, London, p. 1-16.

Bradley, R.S. and Jones, P.D. 1993. "Little Ice Age" summer temperature variations: Their nature and relevance to recent global warming trends. The Holocene, 3,4: 367-376.

Briffa K.R., et al. 1998. Influence of volcanic eruptions on Northern Hemisphere summer temperature over the past 600 years. *Nature* 393: 450-455.

Bryson R.A., and Hare, F.K. 1974. The climates of North America.

Calkin, P.E., Ellis, J.M., Haworth, L.A., and Burns, P.E. 1985. Cirque glacier regime and neoglaciation, Brooks Range, Alaska. *Zeitschrift Für Gletscherkunde und Glazialgeologie* 21: 371-378.

Crowley, T.J. and Kim, K. 1999. Modeling the temperature response to forced climate change over the last six centuries. *Geophysical Research Letters* 26 #13: 1901-1904.

D'Arrigo, R.D., Jacoby, G.C., and Free, R. 1992. Tree-ring width and maximum latewood density at the North American treeline: parameters of climatic change, *Canadian Journal of Forest Research*, 22: 1290-1296.

D'Arrigo, R.D. and Jacoby, G.C. 1993. Secular trends in high northern latitude temperature reconstructions based on tree rings. *Climatic Change* 25: 1-15.

D'Arrigo, R.D. and Jacoby, G.C. 1999. Northern North American tree-ring evidence for regional temperature changes after major volcanic events. *Climatic Change* 41: 1-15.

D'Arrigo, R., Mashig, E., Frank, D., Jacoby, G. and Wilson, R. 2004. Reconstructed warm season temperatures for Nome, Seward Peninsula, Alaska. *Geophysical Research Letters* 31: 1-4.

DeGeer, G. 1912. A geochronology of the last 12,000 years. In, 11th International Geological Congress (1910), Stockholm, Sweden, 1: 241-253.

Desloges, J.R., 1994. Varve deposition and the sediment yield record at three small lakes of the southern Canadian Cordillera. *Arctic and Alpine Research* 26,2: 130-140.

Dronia, H., 1974. Uber temperaturanderungen der freien atmosphare auf der Nordhalbkugel in den letzten 25 jahren. *Meterolol. Rundsch*. 27: 166-174.

Dyurgerov, M.B. and Meier, M.F. 2000. Twentieth century climate change: evidence from small glaciers. *PNAS* 97,4: 1406-1411.

Ellis, J.M. and Calkin, P.E., 1979. Nature and distribution of glaciers, neoglacial moraines, and rock glaciers, east-central Brooks Range, Alaska. *Arctic and Alpine Research* 11,4: 403-420.

Ellis, J.M. and Calkin, P.E., 1984. Chronology of Holocene glaciation, central Brooks Range, Alaska. *Geological Society of America Bulletin* 95: 897-912.

Fischer, H., Werner, M., Wagenbach, D., Schwager, M., Thorsteinnson, T., Wilhelms, F., Kipsftuhl J., and Sommer, S., 1998. Little ice age clearly recorded in northern Greenland ice cores. *Geophysical Research Letters* 25: 1749-1752.

Fisher D.A., 1977. Melt feature stratigraphy, oxygen isotope ratio and climate over 800 years, from the Devon Ice Cap cores. Internal Report of Polar Continental Shelf Project, Energy Mines and Resources, Canada, 35 pp.

Francus, P. and Asikainen C.A., 2001. Sub-sampling unconsolidated sediments: a solution for the preparation of undisturbed thin-sections from clay-rich sediments. *Journal of Paleolimnology* 26: 323-326.

Francus, P., Keimig, F., and Besonen, M., 2002a. An algorithm to aid varve counting and measurement from thin-sections. *Journal of Paleolimnology* 28: 283-286.

Francus, P., Bradley, R.S., Abbott, M.B., Patridge, W., Keimig, F. 2002b. Paleoclimate studies of minerogenic sediments using annually resolved textural parameters. *Geophysical Research Letters* 19, 1998-2001.

Fritts, H.C., 1976. Tree Rings and Climate. Academic Press, New York, 567 pp.

Jouzel, J., Merlivat, L., Petit, J.R., and Lorius, C. 1983. Climatic information over the last century deduced from a detailed isotopic record in the South Pole Snow. *Journal of Geophysical Research*, 88, C4, 2693-2703.

Hardy, D.R., Bradley, R.S., and Zolitschka, B. 1996. The climatic signal in varved sediments from Lake C2, northern Ellesmere Island, Canada. *Journal of Paleolimnology* 16: 227-238.

Hardy, D.R. 1996. Climatic influences on streamflow and sediment flux into Lake C2, northern Ellesmere Island, Canada. *Journal of Paleolimnology* 16: 133-149.

Hardy, D.R. 1992. Arctic runoff and sediment transfer: What is the climate signal? Proceedings: 22nd Arctic Workshop, Andrews, J.T., ed.), Occasional Paper, INSTAAR, Boulder, Colorado, p. 62.

Hattersley-Smith, G. 1973. An archeological site on the north coast of Ellesmere Island. *Arctic* 26: 255-256.

Haugen, R.K. 1982. Climate of remote areas in North-Central Alaska: 1975-1979 Summary. U.S. Army Cold Regions Research and Engineering Laboratory (CRREL) Report 82-35, Hanover, NH.

Hermanson, M.H., 1990. ^{210}Pb and ^{137}Cs chronology of sediments from small, shallow Arctic lakes. *Geochimica et Cosmochimica Acta*, 54: 1443-1451.

Hughen K.A., Overpeck, J.T., Anderson, R.F., and Williams, K.M., 1996. The potential for paleoclimatic records from varved Arctic lake sediments: Baffin Island, Eastern Canadian Arctic, *In* "Palaeoclimatology and Palaeoceanography from Laminated Sediments" (Kemp, A.E.S., Ed.), Geological Society Special Publication 116, London, The Geological Society, pp. 57-71.

Hughen, K.A., Overpeck, J.T. and Anderson, R.F. 2000. Recent warming in a 500-year palaeotemperature record from varved sediments, Upper Soper Lake, Baffin Island, Canada. *The Holocene*10,1: 9-19.

IPCC 2001: Climate Change 2001: The scientific basis : contribution of Working Group I to the third assessment report of Intergovernmental Panel on Climate Change (Houghton, J.T., Ding Y., Griggs D.J., Noguer M., van der Linden P.J., Da X., Maskell K. and Johnson C.A., Eds.) Cambridge University Press, Cambridge, UK., 881 pp.

Indermuhle, A., Stocker, T.F., Joos, F., Fischer, H., Smith, H.J., Wahlen, M., Deck, B., Mastroianni, D., Tschumi, J., Blunier, T., Meyer, R., and Stauffer, B., 1999, Holocene carbon-cycle dynamics based on CO_2 trapped in ice at Taylor Dome, Antarctica: *Nature* 398: 121-125.

Jacoby G.C. and D'Arrigo, R. 1989. Reconstructed Northern Hemisphere annual temperature since 1671 based on high-latitude tree-ring data from North America. *Climate Change* 14: 39-59.

Jacoby G.C., Workman, K.W., and D'Arrigo R.D. 1999. Laki Eruption of 1783, tree rings, and disaster for northwest Alaska Inuit. *Quaternary Science Reviews* 18: 1365-1371.

Jouzel, J., Merlivat, L., Petit, J.R., and Lorius, C., 1983. Climatic information over the last century deduced from a detailed isotopic record in the South Pole snow. *Journal of Geophysical Research* 88, C4: 2693-2703.

Koerner, R.M. 1977. Devon Island ice cap: core stratigraphy and paleoclimate. *Science* 196: 15-18.

Koerner, R.M. and Fisher, D.A., 1990. A record of Holocene summer climate from a Canadian High-Arctic ice core. *Nature* 343: 630-631.

Koerner, R.M. and Lundgaard, 1995. Glaciers and global warming. *Geographie physizue et Quaternaire* 19 3, 429-434.

Krinsley, D., et al. 1998. Backscattered Scanning Electron Microscopy and Image Analysis of Sediments and Sedimentary Rocks, Cambridge, UK; New York: Cambridge University Press

Lamb, H.H., 1995. Climate, History, and the Modern World, New York: Routledge.

Lamoureux, S.F., 1994. Embedding unfrozen lake sediments for thin section preparation. *Journal of Paleolimnology* 10: 141-146.

Lamoureux, S.F. and Bradley R.S. 1996. A late Holocene varved sediment record of environmental change from northern Ellesmere Island, Canada. *Journal of Paleolimnology* 16: 239-255.

Lamoureux, S.F. 1999. Catchment and lake controls over the formation of varves in monomictic Nicolay Lake, Cornwall Island, Nanuvut. *Canadian Journal of Earth Science* 36: 1533-1546.

Lamoureux, S. 2000. Five centuries of interannual sediment yield and rainfall-induced erosion in the Canadian High Arctic recorded in lacustrine varves. *Water Resources Research* 361: 309-318.

Lamoureux, S.F., and Gilbert, R. 2004. A 750-yr record of autumn snowfall and temperature variability and winter storminess recorded in the varved sediments of Bear Lake, Devon Island, Arctic Canada. *Quaternary Research* 61: 134-147.

Leeman A. and Niessen, F. 1994. Varve formation and the climatic record in an Alpine proglacial lake: Calibrating annually-laminated sediments against hydrological and meteorological data. *The Holocene* 4: 1-8.

Lemmen D.S., 1989. The last glaciation of Marvin Peninsula, northern Ellesmere Island, High Arctic, Canada. *Canadian Journal of Earth Sciences* 26: 2578-2590.

Leonard, E.M. 1986. Varve studies at Hector Lake, Alberta, Canada, and relationship between glacial activity and sedimentation. *Quaternary Research* 25: 199-214.

Leonard, E.M. 1997. The relationship between glacial activity and sediment production: evidence from a 4450-year varve record of neoglacial sedimentation in Hector Lake, Alberta, Canada. *Journal of Paleolimnology* 17: 319-330.

MacDonald, G.M., Felzer, B., Finney, B.P., and Foreman, S.L. 2000. Holocene lake sediment records of Arctic hydrology. *Journal of Paleolimnology* 24, 1-14.

Mann, M.E. and Jones, P.D., 2003. 2,000 Year Hemispheric Multi-proxy Temperature Reconstructions, IGBP PAGES/World Data Center for Paleoclimatology; Data Contribution Series #2003-051. NOAA/NGDC Paleoclimatology Program, Boulder CO, USA.

Mann, M. E., Bradley, R. S. and Hughes, M. K. 1999. Northern hemisphere temperatures during the past millennium: Inferences, uncertainties and limitations. *Geophysical Research Letters* 26: 759-762.

Mann, M.E., Bradley, R.S., and Hughes, M.K., 1998. Global-scale temperature patterns and climate forcing over the past six centuries. *Nature* 392: 779-787.

McGovern, T.H. 1991. Climate, correlation, and causation in Norse Greenland. *Arctic Anthropology* 28: 77-100.

Meese D.A., Gow, A.J., Grootes, P., Mayewski, P.A., Ram, M., Stuiver, M., Taylor, K.C. Waddington, E.D., and Zielinski, G.A. 1994. The accumulation record from the GISP2 core as an indicator of climate change throughout the Holocene. *Science* 266: 1680-1682.

Minnis, P., Harrison, E.F., Stowe, L.L., Gibson, G.G>, Denn, F.M., Doelling, D.R., and Smith Jr. W.L. 1993. Radiative climate forcing by the Mount Pinatubo eruption. *Science* 259: 1411-1415.

Mock, C.J., Bartlein, P.J., and Anderson, P.M. 1998. Atmospheric circulation patterns and spatial climatic variations in Beringia. *International Journal of Climatology* 10: 1085-1104.

Moore, J.J., Hughen, K.A., Miller, G.H., and Overpeck, J.T., 2001. Little Ice Age recorded in summer temperature reconstruction from varved sediments of Donard Lake, Baffin Island, Canada. *Journal of Paleolimnology* 25, 503-517.

Nesje, A. and Dahl, S.O., *Glaciers and environmental change* (Arnold, London, 2000).

Newhall, C.G. and Self, S., 1982. The volcanic explosivity index (VEI): An estimate of explosive magnitude for historical volcanism. Journal of Geophysical Research 87: 1231-1238.

Ojala, A.E.K. and Tiljander, M., 2003. Testing the fidelity of sediment chronology: Comparison of varve and paleomagnetic results from Holocene lake sediments from central Finland. *Quaternary Science Reviews* 22: 1787-1803.

Ostrem, G., Bridge, C.W., and Rannie, W.F., 1967. Glacio-hydrology, discharge and sediment transport in the Decade Glacier Area, Baffin Island, N.W.T.. *Geografiska Annaler* 49A: 268-282.

O'Sullivan, P.E., 1983. Annually-laminated lake sediments and the study of Quaternary environmental changes – a review. *Quaternary Science Reviews* 1: 245-313.

Overpeck, J.T., et al., 1997. Arctic environmental change of the last four centuries. *Science* 278: 1251-1256.

Polysciences Inc. (1986) Spurr Low-viscosity Embedding Media. Polysciences data sheet 127.

Rind, D., 2002. The sun's role in climate variation. *Science* 296: 673-677.

Saarnisto, M., 1986. Annually laminated lake sediments, *In*, Berglund, B.E. (ed.), Handbook of Holocene Palaeocology and Palaeohydrology, pp. 343-370.

Shindell, D.T., Schmidt, G.A., Mann, M.E., Rind, D., and Waple, A. 2001. Solar forcing of regional climate change during the Maunder Minimum. *Science* 294: 2149-2152.

Smith, S.V., Bradley, R.S., and Abbott, M.B. 2004. A 300 year record of environmental change from Lake Tuborg, Ellesmere Island, Nanuvut, Canada. *Journal of Paleolimnology* 00: 1-12.

Solomina O. and Calkin P.E. 2003. Lichenometry as applied to moraines in Alaska, U.S.A., and Kamchatka, Russia. *Arctic, Antarctic, and Alpine Research* 35, 2: 129-143.

Stewart, T.G. and England, J., 1983. Holocene sea-ice variations and paleoenvironmental change, northernmost Ellesmere Island, N.W.T., Canada. *Arctic and Alpine Research* 15: 1-17.

Sturm, M. 1979. Origin and composition of clastic varves. *In* “Moraines and varves” (Schlüchter, C. Ed.), A.A. Balkema, Rotterdam, pp. 281-285.

Stuiver, M., Grootes, P.M., and Braziunas, T.F., 1995. The GISP2 $\delta^{18}O$ climate record of the past 16,500 years and the role of the sun, ocean, and volcanoes. *Quaternary Research* 44: 341-354.

Sutherland, P.D. 1992. Environmental change and prehistory in Arctic Canada. *In* “Arctic Environment: Past, Present and Future” (Woo, M. and Gregor, D.J. Eds.) McMaster University, pp. 139-153.

Thompson, L.G. 1989. Ice-core records with emphasis on the global record of the last 2000 years. *In* “Global Changes of the Past” (Bradley, R.S. Ed.), pp. 201-224.

Wendler, G., and Weller, G. 1974. A heat-balance study of McCall Glacier, Brooks Range, Alaska: A contribution to International Hydrological Decade. *Journal of Glaciology* 10: 31-38.

Whitfield, P.H., Hall, A.W., and Cannon, A.J. 2004. Changes in the seasonal cycle in the circumpolar Arctic, 1976-95: temperature and precipitation. *Arctic* 57,1: 80-93.

Wolfe, A.P., Miller, G.H., Olsen, C.A., Forman, S.L., Doran, P.T., and Holmgren, S.U., (In Press). Geochronology of high latitude lake sediments.

Wright, H.E. Jr. et al. 1984. Piston corers for peat and lake sediments. *Ecology* 65,2: 657-659.

Wright, H.E. Jr., Kutzback, J.E., Webb, T., Ruddiman, W.F., Stret-Perrott, F.A., and Bartlein, P.J. (Eds.), 1993. Global Climates Since the Last Glacial Maximum. University of Minnesota Press, Minneapolis, MN.

Zielinski, G.A., Mayewski, P.A., Meeker, L.D., Whitlow, S. Twickler, M.S., Morrison, M., Meese, D.A., Gow, A.J. and Alley, R.B. 1994. Record of volcanism since 7000 B.C. from the GISP2 Greenland ice core and implications for the volcano-climate system. *Science* 264: 948-952.

Zolitschka, B. 1996a. Recent sedimentation in a high Arctic lake, northern Ellesmere Island, Canada. *Journal of Paleolimnology* 16: 169-186

Zolitschka, B. 1996b. High resolution lacustrine sediments and their potential for paleoclimatic reconstruction. *In* “Climatic variations and forcing mechanisms of the last 2000 years” (Jones, P.D. and Bradley R.S Eds.) NATO ASI Series Vol. I 41

Zolitschka, B. 1998. A 14,000 year sediment yield record from western Germany based on annually laminated lake sediments. *Geomorphology* 22: 1-17.